Production of Residual Nuclides from Tungsten by Proton-Induced Reaction below 72 MeV

Diploma Thesis

By

Abu Salek Md. Fahim Chowdhury
Zentrum für Strahlenschutz und Radioökologie
Universität Hannover
Am Kleinen Felde, 30
D-30167 Hannover, Germany

Supervisor:

Professor Dr. Rolf Michel
Zentrum für Strahlenschutz und Radioökologie
Universität Hannover
Am Kleinen Felde, 30
D-30167 Hannover, Germany

February 2005

Contents

List of Tables

List of Figures

Abstract

Investigations of cross-sections for the production of residual nuclides from tungsten by proton induced reaction were performed at an energy range between 10 to 70 MeV using stacked foil technique by the cyclotron facilities present at the Paul Scherrer Institute, Villigen, Switzerland. The irradiated samples were transported from Villigen to Hannover via Cologne. The samples were evaluated by off line gamma-spectroscopy at the Center for Radiation Protection and Radioecology, University of Hannover, Germany. The measured data contains altogether 67 cross-sections for the production of 4 different residual nuclides which are ^{184}Re, ^{182}Re,^{181}Re and ^{177}Ta. The experimentally obtained data were compared with earlier work and the model calculations using codes AREL and TALYS. This comparison demonstrates the necessity for further improvements of the models and the codes. Phenomenological aspects of residual nuclide production and the capabilities of nuclear models to predict respective cross-sections are described in this thesis.

Chapter 1

1.1 Introduction

The development of the accelerator based technology and the invasion of space, both have raised the need to understand and describe the effects of the interaction of high-energy particles with matter. These effects result in a deceleration of the projectiles, which delivers a part of their energy by interactions with the target atoms. This must be differentiated between reactions, which take place in the electron shells of the atoms and results in excitation or ionization of the atoms. The initial state of the electron casing is restored by the capture of electrons as well as by rearranging processes. It makes a change of the nucleon configuration. Today one knows about 2100 different isotopes of the 81 stable as well as the 31 artificially produced elements in over 2600 variations, which all were produced in nuclear reactions. The time scale, of a nuclear reaction, is too short approximately 10^{-22} to 10^{-16} s. In order to investigate one should use indirect procedures based on the analysis of the reaction products, which are the secondary particles and light cluster such as ^{3}He, ^{4}He, ^{3}H, ^{2}H, ^{7}Be etc. and the residuals staying after the reaction. By the current discussions over the disposal of long-lived, radioactive wastes from nuclear reactors, the produced residuals need more investigations due to safety issues.

1.2. Transmutation of nuclear waste by accelerator driven system

Transmutation has the aim to reduce the radiological impacts of actinides and fission products in the high level waste by nuclear transformation of the troublesome long-lived radionuclides. Assuming that high level waste can be safely enclosed in waste containers for about a millennium, the period of concern begins about 1000 years after the irradiation of the fuel, i.e. at a time when the majority of the fission products have decayed and the radiotoxicity of the high level waste is strongly dominated by actinides. However, the long-lived fission products must also be considered since they are more mobile than the actinides and therefore dominate the long term risk of geologic repositories.

Transmutation of one radionuclide into another is achieved by neutron bombardment in a nuclear reactor or by an accelerator driven device. A high-energy proton beam hitting a heavy

metal target produces shower of neutrons by spallation. The neutrons can cause fission in a subcritical fuel assembly, but unlike a conventional reactor, fission ceases when the accelerator is turned off. The fuel may be uranium, plutonium or thorium, possibly mixed with long-lived wastes from conventional reactors. The objective is to change the long-lived actinides and fission products into significantly shorter-lived nuclides. The goal is to have wastes which become radiologically innocuous in only a few hundred years.

Some radiotoxic nuclides, such as ^{239}Pu and the long-lived fission products ^{99}Tc and ^{129}I, can be transmuted (fissioned, in the case of ^{239}Pu) with thermal (slow) neutrons. The minor actinides Np, Am and Cm (as well as the higher isotopes of plutonium) are all highly radiotoxic and much more readily destroyed by fissioning in a fast neutron energy spectrum, where they can also contribute to the generation of power. With repeated recycle in a transmutation system, the radiotoxicity of the spent nuclear fuel can be reduced to the point that after a decay period of less than 1000 years, it is less toxic than the uranium that is originally used to produce the fuel. The need for a waste repository is certainly not eliminated but the hazard posed by the disposed waste materials is greatly reduced.

There is an approach for commercial nuclear energy production without a long term high level waste stream and for transmutation of both fission product and higher actinide commercial waste using a thermal flux of neutrons in the 10^{16} n/cm^{2}s range which can be produced using high-current radio-frequency proton accelerators in the 0.8 to 1.6 GeV energy range. With the recent advances in the proton accelerator technology it is possible to get such high flux, which is approximately 100 times larger than that produced in the typically available thermal reactor. When these protons strike a target of a heavy nuclide with a large radius such as lead, approximately 55 neutrons are generated per proton [Ri89], [Ju86]. The energy deposited for this process is about 30 MeV of proton energy per neutron compared with about 200 MeV of fission energy deposited per useful neutron from a chain reaction in fissile material such as ^{235}U. This large flux of thermal neutrons makes a possible waste inventory in the transmutation system which is smaller by about a factor of 100 than the competing concepts. The accelerator allows the system to operate well below criticality so that the possibility for a criticality accident is eliminated. The elimination of the use of control rods makes this process more convenient

The main constraint on any practical reactor is the use of the available neutrons per fission primarily for maintaining the chain reaction and secondarily for other purposes. The extra neutron produced per fission with an accelerator can be used to transmute waste in addition to keeping the chain reaction on and also for breeding. Consider the case of ^{237}Np. In a high neutron flux, with the capture of two neutrons the target nucleus ^{237}Np produces ^{239}Np by fission which is accompanied the emission of about 2.7 neutrons. So that ^{237}Np behaves as a fuel in high flux. In a lower flux the nucleus ^{238}Np decay to non-fissile ^{238}Pu before the second neutron can be captured. The nucleus may be destroyed by the fission of ^{239}Pu with the release of 2.9 neutrons. On average about four neutrons are needed for destruction in the lower flux. Therefore the ^{237}Np waste is a poison in the low flux but a fuel in the high flux.

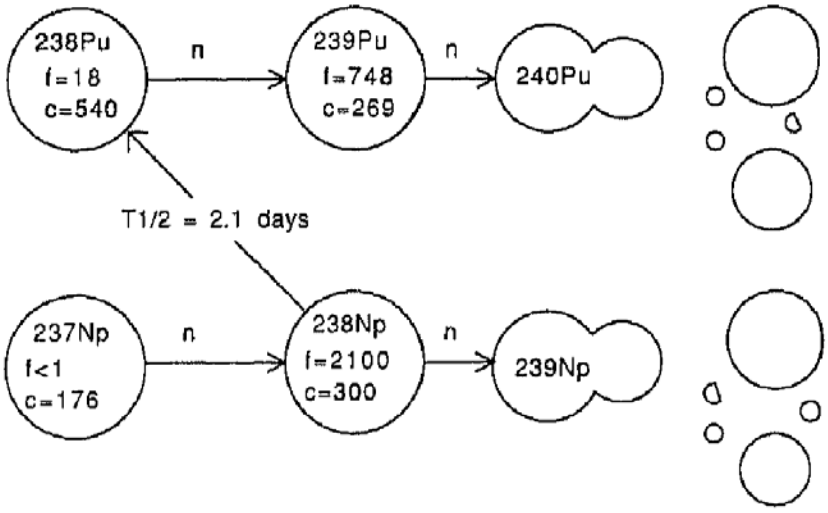

Fig. 1.1: Two step capture process for the higher actinide waste [Bo92]

The two sequences for burning of ^{237}Np in a thermal flux are shown in fig.1.1.

Since the fission cross-section is very low at less than one barn, neutron absorption in ^{237}Np with a 176 b cross-section creates ^{238}Np which decays to ^{238}Pu with a 2.1 day half-life. The fission cross-section for ^{238}Pu is also comparatively small and second neutron absorption leads to ^{239}Pu. The fission cross-section of ^{239}Pu is about three times the capture cross-sections so that about ¾ of the neutron absorptions on ^{239}Pu lead to fission. Thus the fission of ^{237}Np has already costs three neutrons per ^{237}Np nucleus and ¼ of the material still remain to be destroyed by fission. The neutron requirement for thermal fission of a single ^{237}Np nucleus is almost four neutrons which is subsequently more than the number of neutrons emitted in

fission. This inefficient destruction process for a low intensity thermal flux has therefore focused attention on high flux where the capture-to-fission ratio is much more favorable. The large thermal fission cross-section for ^{238}Np of σ = 2088 b along with the higher flux of 1×10^{16} n/cm^2 s gives a 1/(φσ) burn up-period for the nucleus of about 0.5 days. Therefore ^{238}Np will undergo fission most of the time with the absorption of a second neutron before it can decay to ^{238}Pu. About 2.7 neutrons are emitted in the fission process compared to the two absorbed by the ^{237}Np and ^{238}Np, so that the relatively inert ^{237}Np becomes a fuel in a high thermal flux.

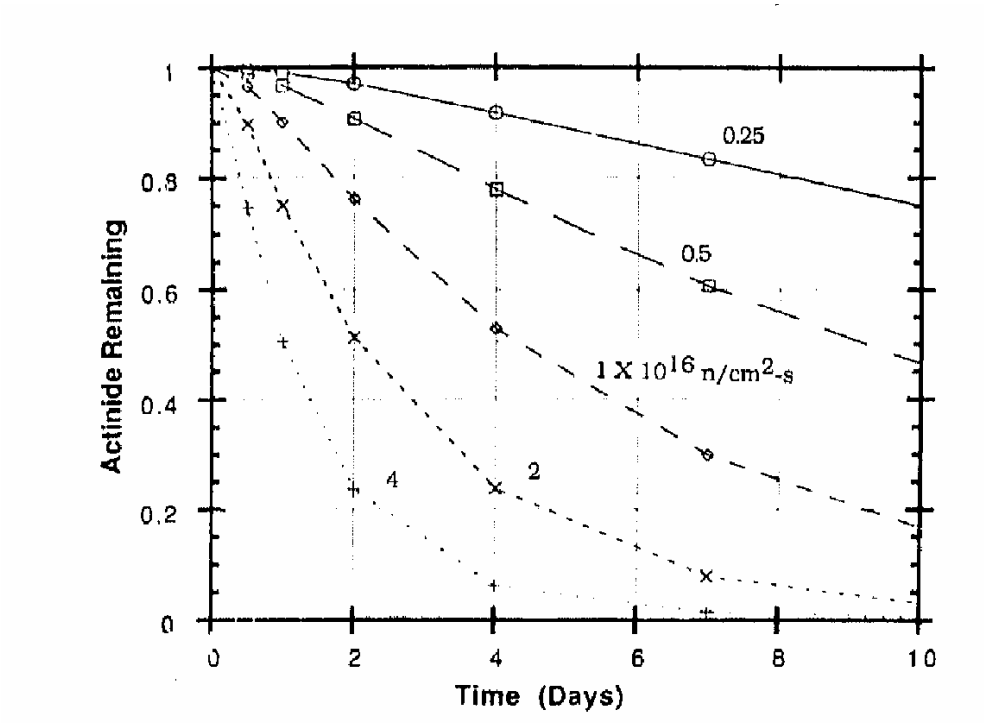

Fig.1.2: Transmutation of ^{237}Np in a high thermal neutron flux. The curves show the amount of actinides remaining as a function of irradiation time. Each curve differs from its neighbours by a factor of two in flux [Bo92].

Fig.1.2 shows transmutation by fission of ^{237}Np for several different fluxes starting from 2.5×10^{15} and progressing by factors of two up to 4×10^{16} n/cm^{2}s. The curves are calculated by using code CINDER [Wi80]

The introduction of accelerator brings six important new features to fission power systems operating with thermal neutrons:

1. The system may operate well below criticality at high power because of the addition of substantial neutrons by accelerator.
2. The effective average number of neutrons per fission can be enhanced as much as 50% with the enhancement adjusted for the particular application.
3. A much higher flux can be produced than is possible in conventional thermal systems since less heat is deposited per neutron produced and the target itself is a flowing medium rather than a fixed medium coolant.
4. The fission products transmutation time is inversely proportional to the flux and this time is reduced by a factor of 100 with an increase in flux by 100, thereby the transmutation of isotopes with low capture cross-section is being possible.
5. The major higher actinide waste constituents ^{241}Am and ^{237}Np are transformed from a poison to a fuel in the high thermal flux.
6. The inventory of waste using this new process is reduced compared to keV-MeV transmutation concepts by a factor of about 100 for the fission products owing to the accelerator driven high thermal neutron flux and by a similar factor for the higher actinides owing to both the high thermal flux and high thermal cross-sections [Bo92].

The other presently available technology is based on the suggestion of Rubbia et al. [Ru95] with the use of external neutron sources. Completely in the sense of the purpose of the existing reactors, they want to use such a system called "Energy Amplification". In a sub-critical reactor, the number of neutrons originating from fission is not sufficient to overcome the losses (due to leaks and absorption of neutrons by some materials). Therefore, under no circumstances a chain reaction can be self-sustained and in order for the reaction to proceed one needs continuous supply of neutrons from an external source. In an accelerator driven system, this external source consists of neutrons created by spallation when a medium energy proton beam reacts with a heavy target (usually lead). The supply of neutrons is proportional to the proton intensity, which can be modified precisely and with a very short time constant. The proton beam plays the role of the control bars in a reactor, the difference being that it is proactive rather than reactive: if it fails, the reaction stops and it can never lead to an overheating.

The energy of an incoming proton initiates nuclear fission cascades and produce much larger energy. Thus it is said to be amplified (by fission) and the device an Energy Amplifier (EA). The ratio between the incoming energy and the total energy is called the gain G of the amplifier. G is related to the neutron multiplication factor k.

$$K = \frac{\text{Production}}{\text{Absorption} + \text{Losses}}$$

In the Energy Amplifier, the transuranic elements coming from the reprocessed spent fuel from a Light Water Reactor will fission and the excess neutrons, captured on the fertile ^{232}Th will breed ^{233}U. An EA of nominal power 1500 MW_{th} with a burn up cycle of 120 GW-day/t refilled after 2 years would incinerate 402 kg of transuranic elements per year, breeding at the same time 175 kg per year of ^{233}U, which can self power a Light Water Reactor [Ca93].

For long-lived fission products, consider as an example ^{99}Tc which is one of the most worrying. By capture of a neutron and subsequent beta decay, it is transformed (after 15 seconds) into stable ^{100}Ru. Since it is not possible to envisage leaving ^{99}Tc in a reactor for hundred years or having a correspondingly high flux. At a slightly higher energy, the capture cross-section of ^{99}Tc shows a series of resonances, the most important one being at 5.6 eV where the cross-section is about three orders of magnitude larger than for thermal neutrons.

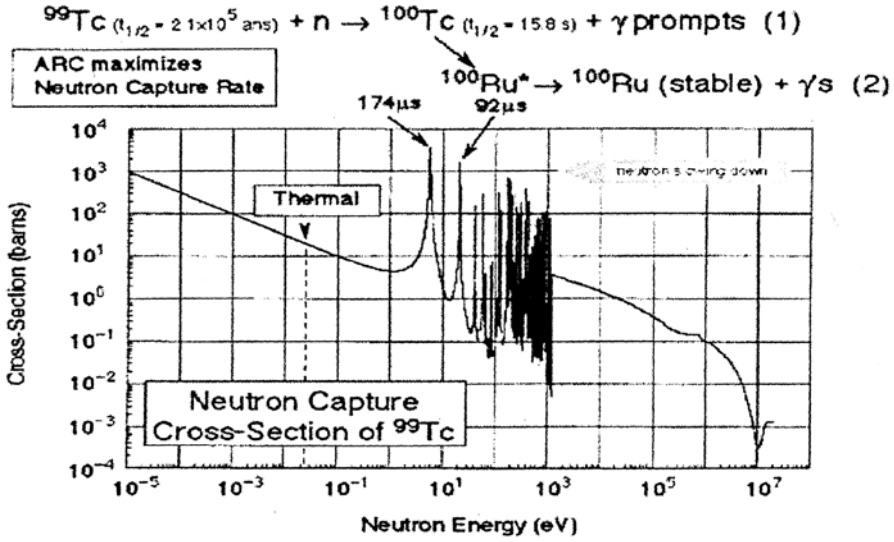

Fig.1.3: Transmutation of ^{99}Tc with a high efficiency using resonances [Kl00]

Consider a volume of Lead bombarded by 1 GeV protons which is large enough to contain the majority of the cascade. A number of neutrons are created and since Lead does not absorb neutrons, they will undergo a large number of elastic collisions and lose their kinetic energy in small decrements governed by the kinematics and the masses. This coefficient which is called lethargy results in the neutron losing at each step a fraction (≈ 1%) of its actual energy. It is easy to see that in the region of the resonances, the actual energy losses are much less than the width of the resonance and therefore, a slowing down neutron cannot miss it. If the impurity that to be destroyed is placed inside a volume where there is no competing absorbing material, it should be destroyed with a high efficiency.

A practical transmutation scheme would locate the technetium at a large distance from the strongly absorbing core, more precisely at a distance larger than the diffusion length of neutrons in Lead. One can safely assume that neutrons that have traveled that far would have a negligible chance of diffusing back to the core. Therefore, one is using for transmutation, neutrons which would otherwise be lost by capture on the wall. This means there is no penalty on energy production. An Energy Amplifier would typically destroy without loss of its own production of technetium. In order to transmute other species (for instance coming from Light Water Reactor waste) one would have to accept a small loss of neutrons, hence of energy production [Ru95].

Accelerator driven transmutation system has opened new possibilities to perform transmutation of nuclear waste addressing some of important concerns related to conventional nuclear power. It relaxes criticality concerns, has a potential for effective transmutation of nuclear wastes including incineration of a Pu-stockpile. Spent fuel from existing Light Water Reactors can be effectively transmuted by the accelerator driven transmutation system, with radioactive waste streams containing virtually no actinides and free of Tc and the long-lived Iodine isotope, i.e. without the most cumbersome isotopes. It opens also new possibilities to design subcritical nuclear power reactors combining transmutation with commercial nuclear energy generation. Development of these transmutation systems requires an extensive research program of interdisciplinary dimensions covering nuclear physics, nuclear technology including high intensity, medium energy accelerators and spallation targets,

reactor physics, material sciences, chemistry and nuclear chemistry, radioactive waste treatment technologies etc.

1.3.1. Cross-sections for the production of residual nuclides

The production of residuals are normally described in terms of cross-section σ that has a unit barn (1 barn $=10^{-28}\,\mathrm{m}^2$). It is a measure of the probability to produce certain residuals R, by the reaction of a projectile p, with a target nucleus T, and depends on the type of the projectile, projectile energy E_p, and on the target nucleus. The reaction is written in the form T(p, x)R, where x is the output channel, which indicates the number as well as the kind of particles that are removed from the target nucleus during the reaction. In order to understand the configuration of the secondary particles in the output channel normally the reaction equation has to be balanced. For example if two protons and two neutrons (x = 2p2n) are emitted in the output channel, then it is stated whether these are emitted individually or for example as an alpha particle.

The production rate P_R of the residual nucleus is normally calculated by

$$P_R = N_T \sigma(E) \phi(E) \tag{1.1}$$

where N_T is the total number of target atoms.

However this is the most artificial case with mono energetic projectile and simple nucleus. Generally the target will be a compound nucleus with n different nucleons, and k different kinds of projectiles. Then the equation (1.1) becomes

$$P_N = \sum_{j=1}^{k} \sum_{i=1}^{n} N_{T_i} \int dE \frac{d\Phi_j(E)}{dE} \sigma_{i.j}(E) \tag{1.2}$$

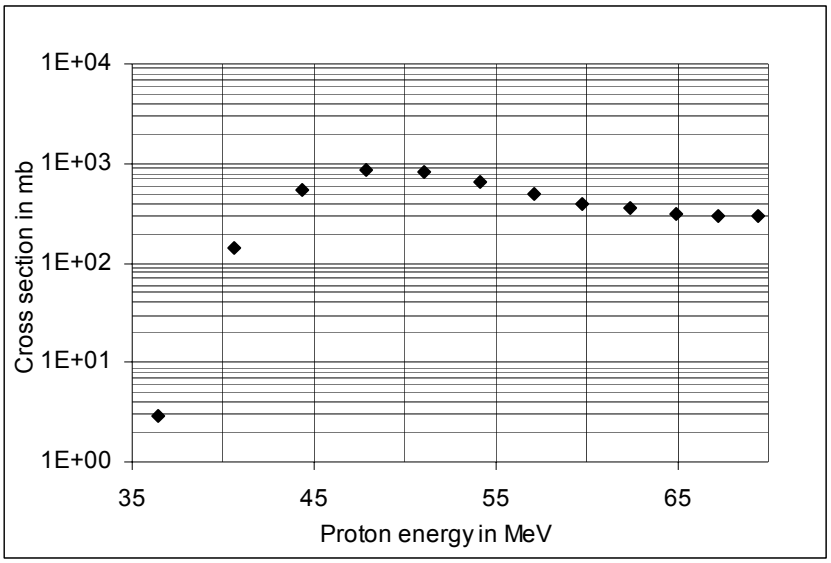

Fig. 1.4: Experimental excitation function for the reaction ^{209}Bi(p,p4n)^{205}Bi [Ul04].

1.3.2 Uses of cross-sections

The cross-section for the production of residual nuclides in nuclear reactions has great significance for a broad diversity of applications. These cross-section data have uses in the study of astro and cosmo-physics, environmental science, medicine (radiation therapy), accelerator technology especially accelerator based nuclear waste transmutation and energy amplification. The target elements under investigation vary due to different particular field of interests. In the field of cosmo-physics, the atomic number $\leq$ 28 of the target elements are of interests. For accelerator based waste transmutation and energy amplification [Kl00], heavy elements with higher atomic numbers are off interests. One of the main concepts of the construction of such devices is the calculation of radioactive inventories of the spallation targets as well as commencement of accelerator parts, shields, cooling media and ambient air. Besides the importance of short-lived radio nuclides, long-lived staffs are also important due to the environmental impacts and problems when these strategies have to be decommissioned and disposed. These areas can be divided into two groups such as, which are under application already for a long time and which are in the recent time.

With the innovation of particle accelerators in the 40's, one encountered the necessity to consider the residuals produced in particle-induced reactions for the first time. The unavoidable beam losses led to an activation of the beam guidance components and thus in contrast,

synchrotron radiation leads to a radiation exposure on the operating personnel by the existing long-lived isotopes. From the knowledge of the cross-sections of the produced radionuclides from different elements, it is able to measure the induced activity and keep it as low as possible. A natural existing radiation source is the cosmic radiation, which predominantly consists of protons with energies up to some GeV. While the atmosphere protects human being to a large extent against the cosmic radiation but it is an additional risk for the astronauts. It activates the spaceship cells and therefore causes a further radiation dose for the astronauts by the decay of induced radioactive nucleus. Pilots of high-flying airplanes are also exposed to the radiation dose caused by the cosmic radiation. A further example of the use of the knowledge about excitation functions is the optimization of the production of radionuclides for medical applications in therapy and diagnostics (radiopharmaceuticals). A total number of different, short-lived nuclides are used for the diagnostic purposes by means of Positron Emission Tomography (PET) and Single Photon Emission Computer Tomography (SPECT). With the knowledge of the production of these nuclides it is tried to find an optimum between a yield of the desired nuclide and as small as possible unwanted nuclides. An overview is given in [Qa97] and [Ko91a].

The treatment of the inaccessible tumours in human body with gamma-radiation and a combination of chemotherapy is very common now a day. For example ^{60}Co sources or bremsstrahlung of the high-energy electrons (up to 70 MeV) is used for this purpose. Since it is difficult to concentrate the irradiation on the affected part of the tissue without making any damage, one can irradiate substantial parts of the healthy tissue for the treatment by means of direct or indirect irradiation. During the direct irradiation with loaded projectiles, the charged particles are very well focused with the help of magnetic fields. Protons are used up to energies of 250 MeV.

1.4 Nuclear reactions

Apart from the experimentally accessible measurement of production cross-sections, the theoretical modelling is necessary in order to understand the nuclear reactions. Beyond that it is also necessary to formulate a model, which is capable in all aspects to describe a reaction.

The theoretical description of nuclear reactions is already a subject under long investigations, nevertheless there is no such a model, which is able to describe the varieties of all the reaction possibilities. A projectile with a mass m_0 and kinetic energy E satisfies the relativistic mass energy relationship

$$m_0c^2 + E = \sqrt{c^2p^2 + m_0^2c^4} \tag{1.3}$$

and the de Broglie wave-length of the particle is

$$\lambda = \frac{h}{p}\frac{hc}{E}\left(1 + \frac{2m_0c^2}{E}\right)^{-1/2} \tag{1.4}$$

The concept of individual nucleon-nucleon interaction led to the development of different models, whose area of application is limited to different energy regions.

At low energy the wave length of the incoming particle is too large that it interacts with the whole nucleus by either direct reaction leading to a change of the nucleus from the initial quantum mechanical energy state to a final quantum mechanical energy state with in one period or lead to the formulation of compound nucleus where the energy of the incoming particle is distributed over all the nucleons within the nucleus and the nucleus reaches a thermodynamically equilibrium state.

When a bombarding particle is absorbed by a nucleus, the kinetic energy of the bombarding particle plus the binding energy released by its capture provides the excitation energy of the compound nucleus. In the compound nucleus model the nucleus is in statistical equilibrium. As the nucleons moves about and collide in the nucleus, their individual kinetic energies vary with each collision. As this process goes on there is an increase in the probability that at least one nucleon will gain kinetic energy in excess of its binding energy. The nucleon is then evaporated. The evaporation of the nucleon decreases the excitation energy of the residual nucleus by an amount corresponding to the binding energy plus the kinetic energy of the released nucleon. The evaporation process continues until the residual excitation energy is less than the binding energy of a nucleon. The excitation energy remaining at this point is removed from the nucleus by the emission of gamma-rays. The nucleons in the compound nucleus is

held together long enough for the energy to be shared by all nucleons. The time required for a nucleon to be evaporated from a compound nucleus is 10^{-16}s [We37]. Since the time is so long and there are so many inter-nucleon collisions that the nucleus loses its memory of the mode of formation. The mode of decay would therefore be independent of the mode of formation and only depends on the amount of excitation energy. The decay of the long-lived compound nucleus is treated by equilibrium statistical mechanics. The compound nucleus theory assumes that the bombarding particle interacts with the nucleus as a whole. The nucleus is excited uniformly and evaporation of low energy nucleons follows. This model fails to explain some of the phenomenon observed as the kinetic energy of the bombarding particle increases. One such observance is the occurrence of high energy neutrons and protons among the emitted particles. Another is the large cross-sections for reactions such as $X_1(p,pxn)X_2$ at energies where 6 or 7 nucleons are evaporated in order to de-excite the nucleus.

Between the direct and compound nucleus there are continuous contributions to the spectra that are explained neither by compound nucleus nor by direct reaction models. The models that formulate the decay into the continuum of a system with an initial partition of projectile energy between relatively few (intrinsic) degrees of freedom, progressing through more complicated configurations until an equilibrium distribution of energy is attained have been called pre-compound or pre-equilibrium model. Pre-equilibrium decay depends on particle mass and energy but independent or slightly dependent on the characteristics of the target nucleus with respect to cross-section. Pre-equilibrium spectra shows strongest forward peaking for the highest energy particles, with a fairly continuous decrease in degree of forward peaking with decreasing energy. Even at low energy particles shows some forward peaking. More details about different models in order to describe pre-equilibrium models are given in chapter 6 and in [Bl75].

At still higher energies compound nucleus formation is too slow to occur at all and the target nucleus (and also projectile in case of heavy ions) splits rapidly into several fragments. The term spallation is often used for reactions in which a number of particles are emitted as a result of a direct interaction. At high bombarding energies above 100MeV/u, high energy protons, neutrons and heavier particles are emitted from the nucleus in a forward direction. Compound nucleus evaporation is expected to be isotopic.

Serber in 1947 [Se47] treated the high-energy reaction as a two-stage process.

(i) During the first stage the nucleons in the incoming particle undergoes direct collision with the individual target nucleons. In these collisions the struck nucleon often receives energy much in excess of its binding energy. Consequently after each collision both the nucleon belonging initially to the bombarding particle and the struck nucleon have the same probability of escaping the nucleus since their kinetic energies are greater than their binding energies. If both particles escape, the nucleus is usually left with only a small amount of excitation energy. This explains the high cross-sections for (p,pn) reactions. Both emitted proton and neutron have large kinetic energies. Either one or both of the original pair may collide with other nucleons in the nucleus rather than escape. During its initial stage, known as knock on cascade process the total number of direct collisions may be one or many. After a period lasting of about 10^{-19}s some of the struck nucleons have left the nucleus.

(ii) In the remaining nucleus the residual excitation energy is uniformly distributed. The reaction then enters in the second and lower stage, during which the residual excitation energy is lost by nucleon evaporation. This stage resembles the compound nucleus system.

In the first phase over nucleon-nucleon interaction between the projectile and the nucleus, the projectile can again interact with other nucleons (cascade). The traversal time of the particle is 10^{-22} s. As the excitation energy of an excited nucleus increases, the energy levels get closer together. Eventually, a continuum is reached where the density of the nuclear levels is so great that it is no longer possible to identify individual levels. When the excited nucleus being at the continuum energy emits a proton or a neutron the resultant nucleus may be still sufficiently energetic that it remains in the continuum region. Due to many particle problems the computation is not possible to perform by analytical way, a model called inter-nuclear cascade evaporation model (INC/E) based on computer code has been developed on the basis of reliable nucleon-nucleon cross-sections. However the complicated fact is, with sufficient high energy of the projectile the nucleon-nucleon interaction produces short-lived radio-nucleus and from their following decay further particles can be produced.

Chapter 2

2. Setting of tasks

Thin target cross-sections for the production of residual nuclides in proton-induced nuclear reactions are necessary for the database which has many applications. The preceding work [Pr97a], [Ul04] supplied cross-sections for tungsten in the medium energy range. The interest for such data based has increased due to the new accelerator-based applications such as "Accelerator Driven Waste Transmutation" and "Accelerator Based Energy Amplification". Elements such as tantalum, tungsten, mercury, lead or bismuth are considered as structure materials for spallation targets in such applications.

For determining the validity of different nuclear models and codes highly reliable experimental data are needed. It was the task of this diploma work to find the cross-sections of the proton induced reaction from tungsten below 72 MeV in context of European Commission's project called HINDAS (High and Intermediate Energy Nuclear Data for Accelerator Driven System) and to complete the excitation functions at lower energies. The irradiation of the target element has to be done by the accelerator facilities at the Paul Scherrer Institute, Villigen, Switzerland with protons energies 45 MeV and 71 MeV. The data has to be evaluated by offline gamma-spectrometry at the Center for Radiation Protection and Radioecology, University of Hannover, Germany.

The cross-sections obtained should be compared with previously obtained experimental data at this energy range and with different theoretical codes based on different nuclear models.

Chapter 3

3. Theoretical concepts for the execution and evaluation of irradiation experiments

In this chapter the theoretical concepts for the execution of the irradiation experiments as well as the measurements and their evaluation are discussed in order to understand the experiment and the discussions.

3.1 Energetic of nuclear reactions

Consider the reaction process

T(p,x)R

In which an incident particle p strikes a target nucleus T brings about a change into a residual nucleus R together with an emitted particle x, and is normally written as

$$T + p = x + R + Q$$

Where Q represents an energy called the reaction energy is included for satisfying the conservation rules for the mass and the energy. If the target nucleus has a charge number Z_T and Z_R is the charge number for the residual then neglecting the binding energy of the atomic electron, the reaction energy Q becomes

$$Q = \Delta E = \{M_T + M_P - M_x - M_R + (Z_T - Z_R)m_e\}u \qquad (3.1)$$

This reaction energy appears as the kinetic energy of the outgoing particle x, together with the recoil energy of the emitted particle R. If $Q>0$ then the reaction is termed as exothermic which corresponds to the liberation of energy and if $Q<0$ then it is called endothermic which

corresponds to the absorption of energy. The threshold energy E_S, starting from which the reaction becomes possible follows as

$$E_S = -\left(1 + \frac{M_P}{M_T}\right) \tag{3.2}$$

Loaded projectiles must overcome the coulomb barrier of the nucleus which is of the form

$$E_C = \frac{Z_P Z_T e^2}{R} \tag{3.3}$$

with $R = r_0 \cdot (A_P^{1/3} + A_T^{1/3})$

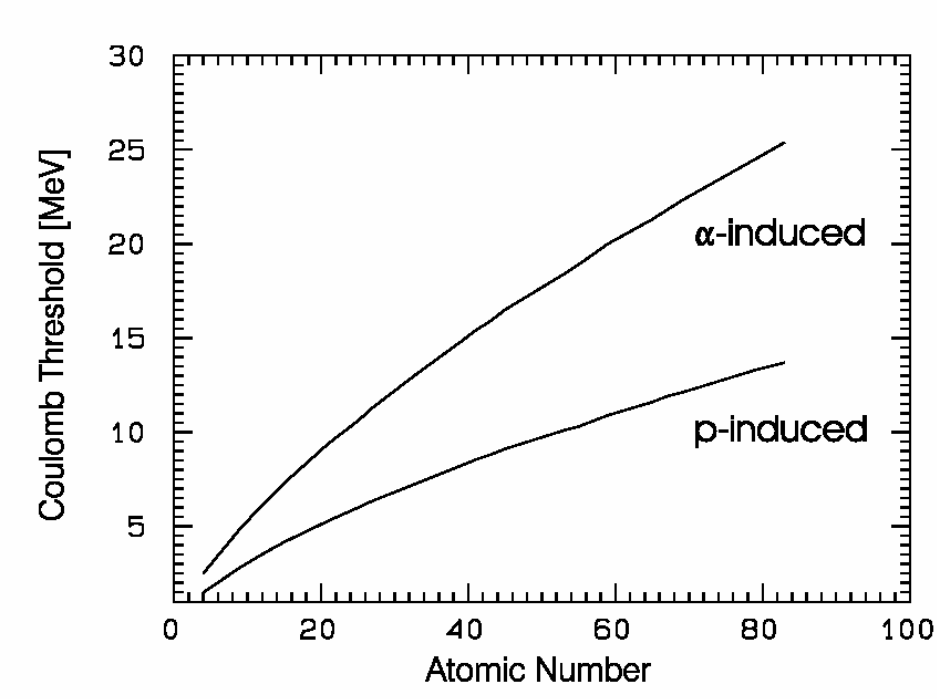

Fig. 3.1: Coulomb barrier for alpha and p-induced reactions.

3.2 Computation of cross-sections

3.2.1 General case

Consider the nuclear reaction T(p, x)R, where a projectile p is incident on the target nucleus T produces the residual R and an emitted particle x. Here ϕ is the projectile flux density. The cross-section σ represents the probability of occurring the reaction. The produced residual nuclide R with half-life $T_{1/2}$ is also radioactive and is subject to the decay law $N(t) = N_0 e^{-\lambda t}$, with decay constant $\lambda = \ln(2)/T_{1/2}$ .The decay rate for the residual is therefore

$$\frac{dN_R}{dt} = \sigma_E \Phi_E N_T - \lambda N_R \tag{3.4}$$

which follows, with the initial condition $N_R(t = 0) = 0$,

$$N_R(t) = \frac{\sigma_E \Phi_E N_T}{\lambda}(1 - e^{-\lambda t}),\ t \le t_{EOI} \tag{3.5}$$

EOI stands for end of the irradiation. At the end of the irradiation with the duration t_{irr} the activity becomes

$$A(t_{EOI}) = \lambda N_R = \sigma_E \Phi_E N_T \left(1 - e^{-\lambda t_{irr}}\right) \tag{3.6}$$

The number of counts C, which is treated as the neat peak area detected by a detector with efficiency $\varepsilon_\gamma(E_\gamma)$ in a full peak of the gamma-energy E_γ that is the number of gamma-quanta emitted by the nucleus with intensity $I_\gamma(E_\gamma)$. C is related with the activity A(t) by

$$C = I_\gamma \varepsilon_\gamma \int_{t_{BOC}}^{t_{EOC}} dt A(t) \tag{3.7}$$

BOC is beginning of counting. The activity of the nuclide at the beginning of the measurement $A(t_{BOC})$ is given by

$$A(t_{BOC}) = \frac{C\lambda}{I_\gamma \varepsilon_\gamma (1 - e^{-\lambda t_C})} \tag{3.8}$$

The time of decay t_d is given by $t_d = t_{BOC} - t_{EOI}$. From equation (3.6) and (3.8) finally the cross-section σ_E is calculated by

$$\sigma_E = \frac{A(t_{EOI})}{\Phi_E N_T (1 - e^{-\lambda t_{irr}})} = \frac{C\lambda}{I_\gamma \varepsilon_\gamma \Phi_E N_T} \cdot \frac{e^{\lambda t_d}}{(1 - e^{-\lambda t_{irr}})(1 - e^{-\lambda t_C})} \tag{3.9}$$

If the cross-section of a reaction is known, then naturally the flux density can be determined by simply transforming the equation (3.9). This is described in details in the chapter 4.

3.2.2 Cumulative cross-section and independent cross-section

While calculating the cross-section of a residual, two types of cross-sections are taken into account. One is independent and the other is cumulative. Equation (3.6) and (3.9) are valid strictly for independent cross-section that is, the residual are produced independently. But in nuclear reactions majority of the cases produce daughter nuclides by β^-, β^+, EC or α-decay of radioactive precursors.

Independent cross-sections are produced if either one of the following conditions is fulfilled

- The nuclei is shielded by stable nuclides against α-decay or by long-lived progenitors (e.g. ^{60}Co by ^{60}Fe with $T_{1/2}$ = 1.5×106 a, or ^{194}Au by ^{194}Hg with $T_{1/2}$ = 520a),

- The cross-section for the production of a progenitor is also measured so that the production via decay can be corrected.

Apart from the above definition cross-sections in all other cases are cumulative, since they include also the production via decay of precursors. This work dealt only with the independent cross-sections.

Chapter 4

4 Experiments and evaluation

In this chapter the experimental procedures represented are based on the theoretical concepts discussed before. At the end a detailed description regarding the uncertainties involved in different procedures are discussed.

4.1 Introduction

The measurement of integral thin target cross-sections for the production of residual nuclides by proton-induced reactions can take place in different ways. For the production of the residual nucleus, either one of the following two different procedures is possible:

- The classical option of the irradiation of a target with protons and neutrons.

- The irradiation of the target element with hydrogen atom, which becomes possible in the recent time by the progressive development in the accelerator technology, Webber et al [We90a], [We90b], [We90c], [We90d], with nuclides from ^{12}C up to ^{58}Ni. This technology is used for heavy ion research at GSI, Darmstadt, Germany [Fa97], [Be01], [En99], [En01], [En02], [Re01].

The latter procedure requires a high experimental expenditure but this gives a more details of the residual nuclides. In this work the classical option of irradiation of the target with protons was used.

The targets can be illuminated with such experiments either in the form of individual foils or directly as a whole foil piles, called "stacks". Both have advantages and disadvantages. During the irradiation of thin single foils, unwanted reactions of secondarily produced particles in the target is neglected, which is not always ensured in massive stacks, depends however on the projectile energy. On the other side, in the case of single foils recoil losses must to be counted and in addition it depends on the projectile flux density problems with the measuring statistics.

If many targets are to be examined, the irradiation of single foils is time consuming and not cost effective. The "stacked foil technique" considers possible secondary particle effects, where the targets are arranged one behind the other and illuminated at the same time. In this work secondary particle effect is not considered because at energies below 200 MeV this is not significant. This technology makes it also possible to determine the cross-sections for several projectile energies because the primary particle meets the targets due to their deceleration in the stack with different energies. Under these considerations, the stacked foil technique is used in this work.

4.2.1 Stack design

The Design of the illuminated stacks depended on the following general criteria:

Avoidance of recoil losses and cross contamination

The loss of activated nucleons from targets due to recoil effects reduced the activities of the target and thus leads to wrong computation of cross-sections. On the other hand at the same time neighbouring targets are contaminated and thus additional or increased activities are pretended.

For this reason a set is always illuminated consisting of at least three targets of the same element, by which the middle is considered for the measurement where the first one shields from the recoil process and the third one shields the other set from cross contamination. Additionally before each target set three monitors were used which also acts as a shield.

Thickness of the targets

The thickness of the targets depends on the manufacturer technical obligations. Targets should be as small as possible with a mass allocation in order to keep the production of secondary particle small.

Stopping power calculations

Since the stacked foil technique is used, the proton energies should be calculated in all the different target foils even though the energy degradation was small for the highest initial proton energies. This was done by a computer program called Stack, originally based on the

work of Andersen and Ziegler [An77]. At high energies the formula for the stopping power shows the dependence on two parameters; the mean ionization potential and the shell correction. These both parameters are different for different materials. The linear stopping power S for charged particles in a target is defined as the differential energy loss for that particle within the material divided by the corresponding differential path length

$$S = -\frac{dE}{dx} \tag{4.1}$$

For particles with a given charged state, S increases as the particle velocity decreases. The specific energy loss for the particle is obtained from the Bethe formula after the shell correction and is given by

$$-\frac{dE}{dx} = \frac{4\pi e^4 Z_p^2}{m_e v^2} N_T Z_T \left[\ln\left(\frac{2mv^2}{I}\right) + \ln\left(\frac{1}{1-\beta^2}\right) - \beta^2 - \frac{C}{Z_T} - \frac{1}{2}\delta \right] \tag{4.2}$$

where,

S is stopping power

e is electron charge

m_e is mass of the electron

Z_p is atomic number of the projectile

Z_T is atomic number of the target

$\beta = v/c$, where v is the velocity of the projectile and c is the velocity of light

C/Z_T is shell correction

I is ionization potential

δ is thickness effect

The dependence of electronic stopping cross-section on the atomic number of the target material has been studied on the basis of binary stopping theory over a wide range of beam energies. This also depends on the atomic number of the target nucleus. This behaviour is caused by the interplay between projectile screening and the closing of inner target shells as a function of velocity [Zi85].

On the basis of equation (4.2) Andersen and Ziegler [An77] developed the parameterized form, which is particularly suitable for computer-assisted calculations:

$$-\frac{dE}{N_T dx} = \frac{A}{\beta^2}\left[\ln\left(B\beta^2\right) - \ln\left(1-\beta^2\right) - \beta^2 - \sum_{t=0}^{4} a_i \left(\ln E\right)^t\right] \tag{4.3}$$

Thus seven coefficients were developed by fits to experimental data of the respective target elements in energy range between 1 MeV to 100 MeV. The descriptions of the parameterization are described by Anderson et al. [An77]. This procedure is also applicable for high proton energies. This was supported by [Fi96] on the work of Ziegler et al. [Zi85].

Since the energy loss *–dE/dt* of the projectiles in an absorber substance is a statistical process; therefore a spread in energies always results after a beam of monoenergetic charged particles has passed through a given thickness of the absorber. This "energy straggling" [Bo15] is a Gaussian distribution, whose width is given by α, which is the energy straggling parameter.

$$\alpha^2 = 4\pi e^4 N_A Z_P^2 \frac{Z_T}{A_T}\xi_T\left[1 + \frac{4I}{3m_e v^2}\ln\left(\frac{2m_e v^2}{I}\right)\right] \tag{4.4}$$

4.2.2 Sample preparation

The targets were supplied by Goodfellow Metals Ltd. U.K. in the form of rectangular foil with a high purity (99.99%) in order to avoid additional production of nuclei from the impurity. The further sample preparation was accomplished exclusively in the Department of Nuclear Chemistry of the University of Cologne. The targets were in circular form with a diameter of 15.0 mm. The thickness of cupper and tungsten foils in the case of irradiation by 45 MeV proton beam was 0.5 mm each and for 71 MeV the thickness of aluminium was 0.125 mm and for cupper and tungsten it was 0.05 mm each. Targets were cleaned and weighted. The masses of the cupper foils in the stack irradiated by 45 MeV proton beam were ranged from 74.05 to 77.3 mg while for the tungsten, it ranged from 157.89 to 162.16 mg. In the case of 71 MeV, the masses of aluminium foils ranged from 57.94 to 59.31 mg. For cupper foil the masses ranged from 73.86 to 79.26 mg and for tungsten it was 149.56 to 164.61 mg. Subsequently the prepared targets were set into the actual sample holders, whereby the irradiation direction and

the composition of the stacks were held. The foils were arranged in two holders, one for 45 MeV and the other for 71 MeV irradiation, where for 45 MeV three cupper targets were arranged in front, followed by three tungsten targets then again three cupper targets and so on. In case of 71 MeV, there were three aluminium, and then three cupper followed by three tungsten then again three cupper and then three tungsten and so on. This was the cycle. The cupper and aluminium foils were used as monitors for measuring the flux densities via monitoring reactions $^{27}Al(p,3p3n)^{22}N$ and $^{65}Cu(p,n)^{65}Zn$ respectively.

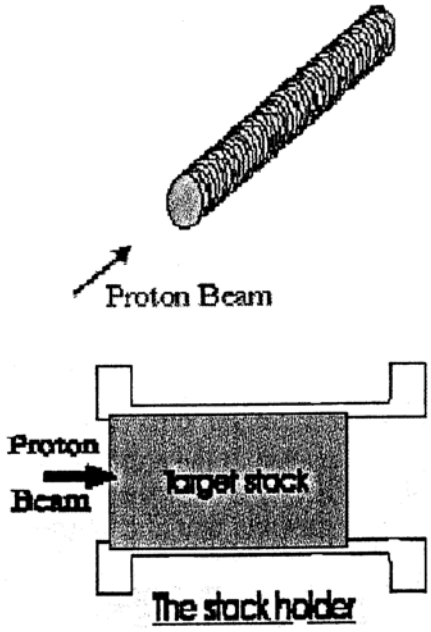

Fig. 4.1: Overview of the stack of target foils and the target holders.

4.2.3 Irradiation at the Paul Scherrer Institute (PSI), Switzerland

The irradiations were performed at the Paul Scherrer Institute, Villigan, Switzerland with Injector-2 cyclotron. Irradiation for the first stack was performed by 71 MeV proton beam for 3 hours and 5 minutes while for the second stack; the irradiation was performed by 45 MeV proton beam for 4 hours and 23 minutes. For each irradiation a protocol was kept in which the beam current or interruptions could be taken into account for the calculation of cross-section. Only the middle one of the Cu, Al and W among the three in the arrangements was taken into account in order to avoid recoil loss and cross contamination.

4.3 Gamma – spectrometry

After the irradiation the stacks were transported to Hannover for offline gamma-spectroscopy. A general introduction for gamma-spectroscopy is described here.

4.3.1 Introduction

Gamma-quanta are usually emitted by the decay of a nucleus and possess energy characteristics of the nucleus and can be detected by means of suitable detectors over their interaction with the subject. Semiconductor crystals, e.g. Si(Li), Ge(Li) or HPGe (High Purity Germanium) are used to form the core of the detectors. The interaction of gamma-rays with the detector core produces free charge carriers. Although a large number of possible interaction mechanisms are known for interaction of gamma-rays with matter, only photo-electric absorption, Compton scattering and pair production, these three types play major roles in radiation measurements. The charge produced with complete absorption of a photon in the crystal is proportional to the energy of the quantum. It can be converted into impulses via amplifiers. These again can be digitized with analogue-digital converters (ADC) and be assigned according to their sizes in different channels of a multi-channel buffers (MCB).

The gamma-quanta is Gauss-shaped distribution in the spectrum due to the statistics of the charge production process as well as the electronic noise [De88] assigned with. This is called "full energy peak". Deviations from the Gaussian shape which results from incomplete charge collection in the crystal and become apparent on the low-energy side of the peaks is called "low energy tailing" while "high energy tailing" that can be normally avoided occurs due to high counting rates from pile up effects. During diminishing away of an impulse in the amplifier another one is overlaid, so that the two impulses cannot to be clearly separated any longer and this causes deviations from the Gaussian shape of the peak on the high-energy side of the spectrum.

More detailed description of the detector systems is given in the text book literature [De88].

4.3.2 Measuring systems at the ZSR

The measurements were made with Ge(Li) detector connected with an automatic sample changer system where up to 16 samples can be kept at a time and measured successively for several times automatically. The samples are kept in a roundabout which is four meters away from the detector. The detector is shielded with 10 cm thick lead, so that outside radiation does not affect the measurement. The detector is movable and it can be positioned at different distances from the sample.

The detector is connected via spectroscopic amplifier to the computer controlled multi-channel buffer (MCB). The built in ADC (analogue digital converter) digitalized the received pulses into spectra. The amplification was chosen for the registration of gamma-quanta with energies between some keV to about 2 MeV. Typical resolution ranged from about 1 keV at 122 keV of ^{57}Co to about 2 keV at 1332 keV of ^{60}Co. The ADC measured the counting time t_C, and also the life time t_L during the impulses were actually digitized, so that from these information the dead time could be computed by $t_D = t_C - t_L$. The spectra is viewed in the computer screen and it is stored together with information of the illuminated sample, e.g. name of the detector, measuring geometry, energy calibration as well as measuring time and life time in a standard format for further processing.

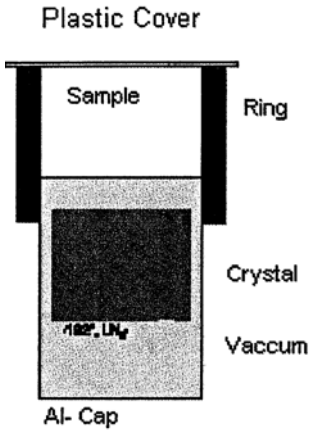

Fig. 4.2: Perpendicular cross-section of used standard geometry

4.3.3 Resolution of the detector

The dominant characteristic of germanium detectors is their excellent energy resolution when applied to gamma-ray spectroscopy. The great superiority of the germanium system is that the energy resolution allows the separation of many closely spaced gamma-ray energies, which remain unresolved in the NaI(TI) spectrum. Virtually all gamma-ray spectroscopy that involves complex energy spectra is carried out with germanium detectors.

Overall energy resolution for a germanium detector is normally determined by a combination of three factors, the inherent statistical spread in the number of charge carriers, variations in the charge collection efficiency and contribution of electronic noise. The energy of the radiation, the size and the quality of the detector determines which of the following three factors will dominate.

The full width at half maximum (FWHM), W_T, of a typical peak in the detection of a mono-energetic gamma-ray can be synthesized as follows [Kn00],

$$W_T^2 = W_D^2 + W_X^2 + W_E^2 \tag{4.13}$$

Where W values on the right hand side are the peak widths that would be observed due to the effects of carrier statistics, charge collection, and electronic noise. The first of these factors; W_D^2, represents the inherent fluctuation in the number of charge carriers created and is given by

$$W_D^2 = (2.35)^2 F \varepsilon E \tag{4.14}$$

Where F, is the Fano factor, ε, is the energy necessary to create one electron hole pair, and E, is the gamma-ray energy.

The contribution of the second term, W_X^2, is due to incomplete charge collection and is most significant in detectors of large volume and low average energy field. Its magnitude can often be experimentally estimated by carrying out a series of FWHM measurements as the applied voltage is varied. The assumption is that, if the electric field could be made infinitely large, the effects of incomplete charge collection could be reduced to an insignificant level.

The third factor, W_E^2, represents the broadening effects of all electronic components following the detector. Its magnitude can conveniently measured by supplying the output of a precision pulser with highly stable amplitude to the preamplifier so that capacitive loading of the preamplifier is normally provided for this purpose.

4.3.4 Energy calibration

In gamma-ray spectroscopy with germanium detectors, the pulse height scale must be calibrated in terms of absolute gamma-ray energy if various peaks in the spectrum are to be properly identified. In many routine applications, the gamma-rays expected to appear in the spectrums are well known in advance and the corresponding peaks can readily be identified by inspection. In other applications, unknown gamma-ray spectra may be encountered which do not provide an unambiguous calibration of energy scale. In such cases, a separated calibration gamma-ray source is conventionally used to supply peaks of known energy in the spectrum. Accurate calibration should involve a standard source with gamma-ray energies that are not widely different from those to be measured in the unknown spectrum. Because even the best spectrometer systems often show nonlinearities of a channel or two over a full range of several thousand channels, it is also useful to have multiple calibration peaks at various points along the measured energy range to account for these nonlinearities.

The precision to which the centroid of a peak in a pulse height spectrum can be localized depends on the spectrometer system resolution and its stability over the period of the measurement. With high-quality germanium system, the uncertainty in the peak position can approach one part in 10^5, which is of the same order as the uncertainty in the calibration energy standards. Therefore, an important goal is to define closely the energy of the standards so that their energy uncertainty does not contribute unnecessarily to the overall imprecision of the gamma-ray measurement. Here standard sources which were ^{241}Am and ^{152}Eu certified by Physikalisch-Technische Bundesanstalt (PTB) at Braunschweig, were used for energy calibration. This was done by the commercially available software GAMMA-W. Excellent agreements between the experimental and certified values were obtained. These calibration parameters were stored in a file and frequently used in all evaluation of the spectrum by GAMMA-W.

4.3.5 Efficiency calibration

For the measurement of activity of the radionuclide, knowledge of the detector efficiency is necessary. All radiation detectors will, in principle give rise to an output pulse for each quantum of radiation that interacts with its active volume. For primary charged radiation such as alpha or beta particles, interaction in the form of ionization or excitation will take place immediately upon entry of the particle in the detector's active volume. After travelling a small fraction of its range, a typical particle will form enough ion pairs along its path to ensure that the resulting pulse is large enough to be recorded. Thus it is often easy to arrange a situation in which a detector will see every particle that enters into its active volume. Under these conditions, the detector is said to have a counting efficiency of 100%. On the other hand uncharged radiations such as gamma-rays or neutrons must undergo a significant interaction with the detector before detection is possible. Because these radiations can travel a large distance between interactions, detectors are often less than 100% efficient. It is then necessary to have precise figure for the detector efficiency in order to relate the number of pulses counted to the number of neutrons or photons incident on the detector. According to the dependence, the efficiencies of the detectors are divided into two categories; absolute efficiency and intrinsic efficiency. Where absolute efficiency is defined as

$$\varepsilon = \frac{\text{Number of pulses recorded}}{\text{Number of radiation quanta emitted by the source}} \tag{5.15}$$

and depends not only on the detector properties but also on the details of the counting geometries (the distance from the source to the detector). The intrinsic efficiency is defined as

$$\varepsilon = \frac{\text{Number of pulses recorded}}{\text{Number of radiation quanta incident on the detector}} \tag{4.16}$$

and no longer includes the solid angle subtended by the detector as an implicit factor. For isotopic sources, the two efficiencies are related by

$$\varepsilon_{\text{int}} = \varepsilon_{abs} \cdot (4\pi / \Omega) \tag{4.17}$$

Where Ω, is the solid angle of the detector seen from the actual source position. If the coincidence detection probability of the two gamma-rays is neglected, then one can calculate the factor by the product of two probabilities in a nuclear decay, the probability that a gamma-ray of energy E_g is emitted and the probability of registration of this gamma-ray in the spectrum with full energy peak. The emission probability can be obtained from the properties of the radioactive nuclei. The detection probability is then defined as

$$\varepsilon = \frac{\text{Number of detected photons}}{\text{Number of emitted photons}} \tag{4.18}$$

This is usually defined as the experimental efficiency and depends on the detector properties, sample properties and the relative sample-detector position. Experimental efficiency must be known in order to measure the activities of a sample. The uncertainty in the counting efficiency is the main source of uncertainties in the calculation of the activity.

Standard point sources which were ^{241}Am and ^{152}Eu and standard solution source which contains ^{241}Am, ^{109}Cd, ^{57}Co, ^{139}Ce, ^{203}Hg, ^{113}Sn, ^{85}Sr, ^{137}Cs, ^{88}Y, and ^{60}Co certified by Physikalisch-Technische Bundesanstalt (PTB) at Braunschweig with known activities and half-lives were used to measure the efficiencies of the detector at geometries 0 cm, 5 cm, 10 cm, 15 cm and 20 cm as gamma-spectrometric measurements for the target samples were performed at these distances due to dead time considerations. Fig. 4.3 and 4.4 show the efficiency calibration of the detector at different geometries for standard point source and standard solution source respectively. Fig. 4.5 shows the comparison between the different sources which exhibit the consistency of the efficiency due to different sources. The efficiencies were calculated by using the formula

$$\varepsilon_{eff} = \frac{N_p \cdot 100}{I_\gamma \cdot t_d \cdot A_{ref} . e^{-\lambda \cdot t_c}} \tag{4.19}$$

where,

N_p is the net peak area

I_γ is the intensity of the gamma-energy line in %

t_D is the time of decay

A_{ref} is the activity of the standard source at the reference date.

t_c is the time of count

λ is the decay constant.

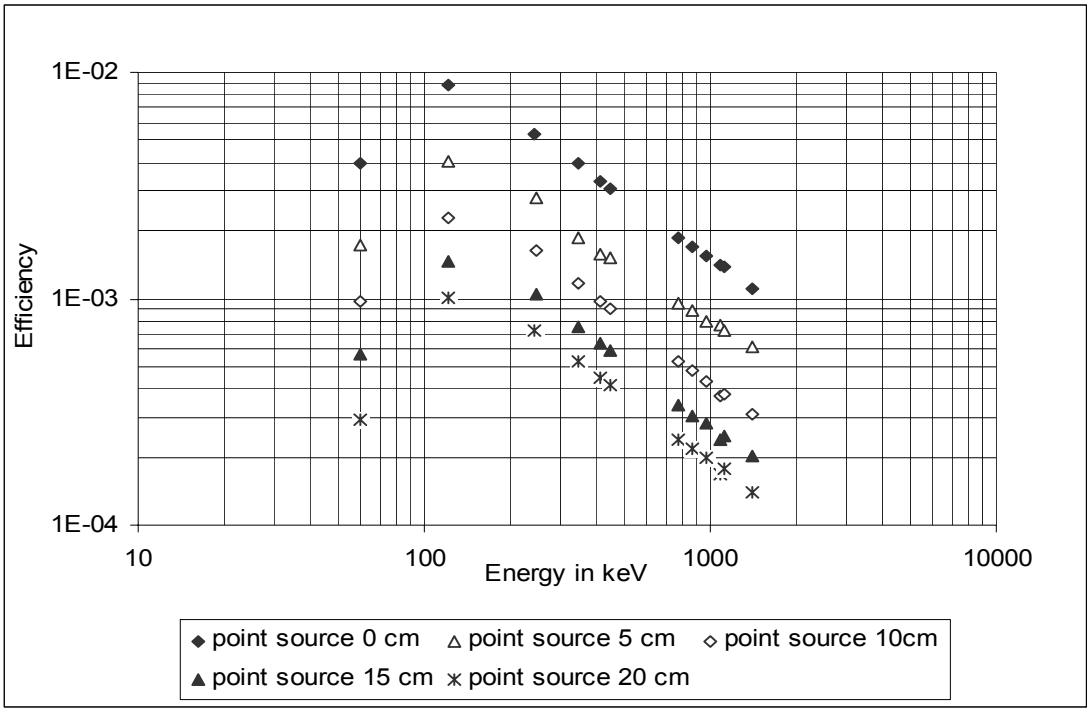

Fig. 4.3: Experimental efficiency of the detector with point sources in different geometries

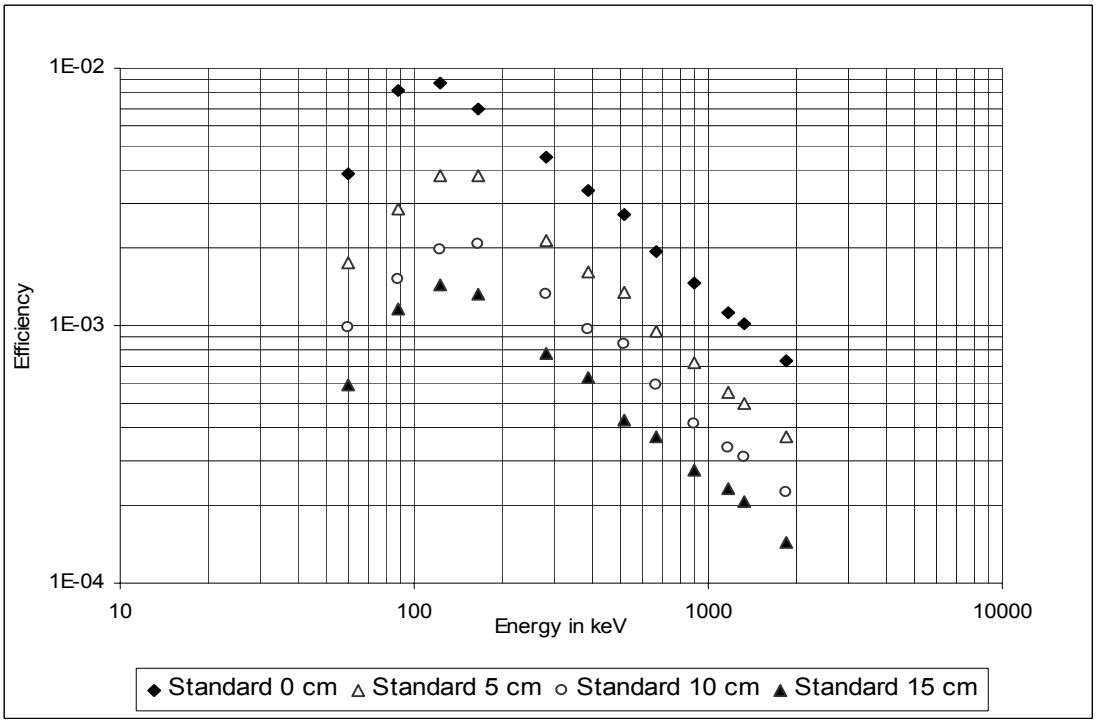

Fig. 4.4: Experimental efficiency of the detector with standard solution sources in different geometries

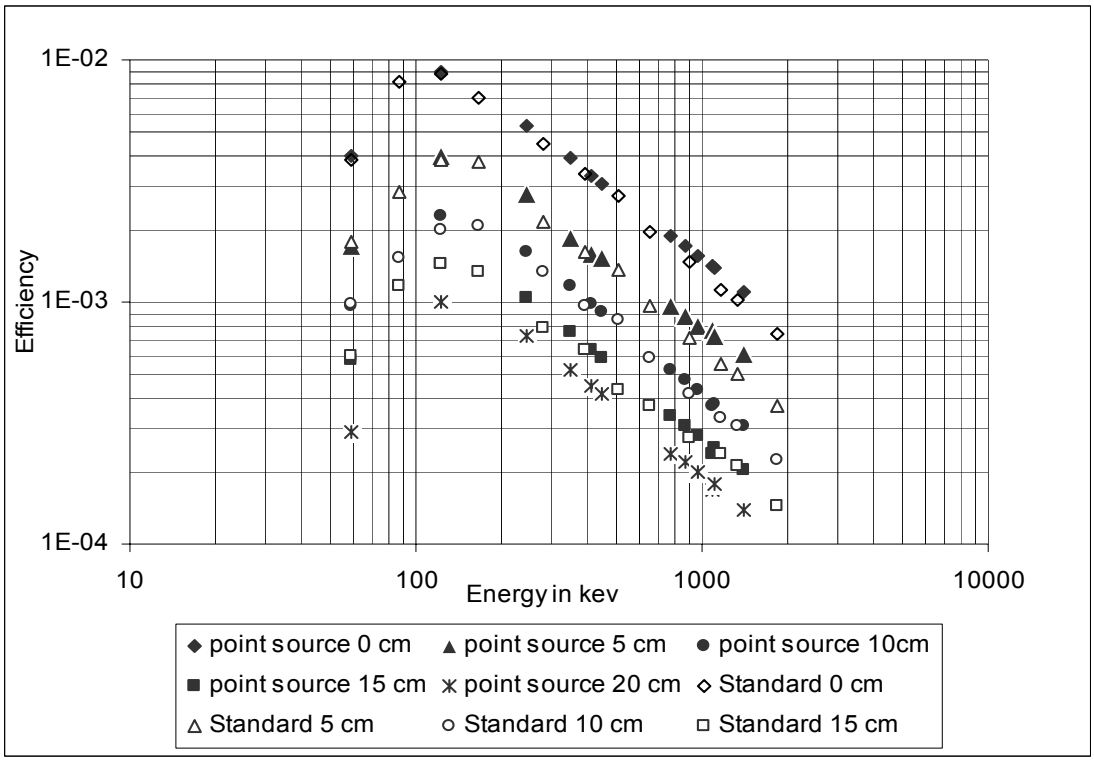

Fig. 4.5: Comparison of the experimental efficiency of the detector between point source and standard solution source in different geometries

For the evaluation of the efficiencies, the linear fit function provided by Microsoft Excel ® was used which is a 5th order polynomial of the form

$$\varepsilon_{eff} = \exp\left[\sum_{i=1}^{5} a_i (\ln E_\gamma)^5\right] \tag{4.20}$$

This equation determines the absolute efficiencies, where E_γ is the energy of the gamma-line of the sample and a_i is the fit parameter. Efficiency calibration for the standard point source is considered here for obtaining the fitting function as it exhibits better results than standard solution.

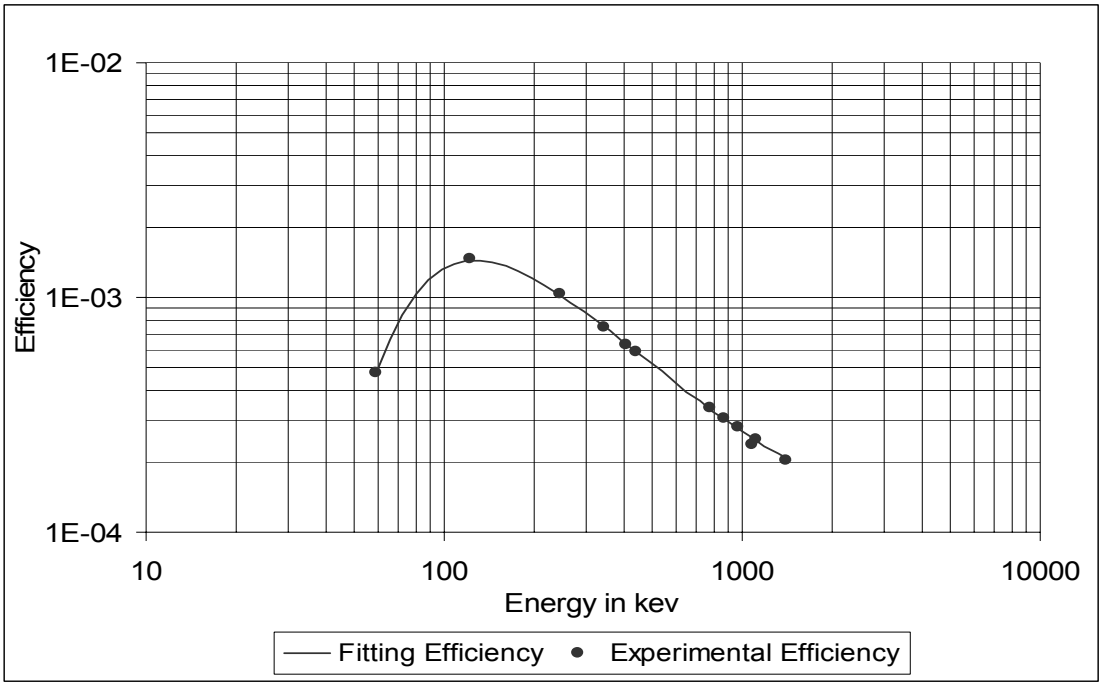

Fig.4.6: Comparison of experimental efficiency with fitting efficiency at geometry of 15 cm

4.3.6 Nomenclature and measurements

Because of the time duration due to transport of the sample from the PSI, Switzerland over Cologne to Hannover, the first spectrometric measurement of the stacks was accomplished not before than 36 hours after the irradiation. The samples were unpacked from the holder and kept on plastic cards where the names of the samples were written according to the arrangement by the program stack. The names include seven letters. First two letters were for name of the element such as CU for cupper, WW for tungsten, AL for aluminium. Then CA or CB. CA stands for sample from the stack which was irradiated by 45 MeV proton beam and CB for the samples of the stack irradiated by 71 MeV proton beam. Then there was a "0". The sixth letter was allocated for the position of the set of each individual element. The first set composed of three samples of cupper in the case of 45 MeV followed by a set of three tungsten and then again a set of cupper and so on. So cupper was the first element. It was "1" in the sixth letter for first set of cupper then "2" for the second set and so on. Same procedure followed for other elements. The 7^{th} letter was for the numbering according to the position of the sample in each set. For the first set of copper it was 1, 2 and 3 respectively and the same procedure followed for the rest. Thus the names were

CUCA011

CUCA012
CUCA013
WWCA011
WWCA012
WWCA013
CUCA021
CUCA022
CUCA023
WWCA021
and so on.

Only the middle of each three samples was considered for the measurement in order to avoid recoil loss and cross contamination as discussed before. In total there were 17 samples of tungsten which were 8 from the stack irradiated by 45 MeV proton beam, 9 from the stack irradiated by 71 MeV proton beam. For monitor there were 19 cupper samples where 9 from the stack irradiated by 45 MeV proton beam and 10 from the stack irradiated by 71 MeV proton beam. There were 5 aluminium samples from the stack irradiated by 71 MeV proton beam. The monitors were kept in small plastic boxes along with their name written on the box and they were put in the store for later measurement. In the automatic sample changer it was possible to keep 16 samples at a time which can be measured according to the user preferred time. Thus from both stacks 8 samples each were kept in the sample changer for measurement. The names of the samples again had to be mentioned in the computer program. But this time the procedure was different. Here 8 letters were allocated for the name for each measurement. The first two letters were normally given according to measuring geometry as 00 for 0 cm distance of the sample from the detector. While next four letters were computer default according to the date of measuring. The first two were for day and the second two were for month. The last two were again given by the user. Normally this is used in order to mention the position of the sample in the sample changer. Thus the name takes the form e.g. 00250401. From this name it is possible to understand that the sample was measured in the 25^{th} of April at geometry of 0 cm from the detector and the sample was at the 1^{st} position in the changer. Additional information can be written in the log file. The samples were arranged in the sample changer according to the sequence they were kept for irradiation. They were measured for 1 hour, 3 hours and 5 hours. Several measurements were made in different geometries. The maximum dead time allowed was 10% because pile up effect accompanies the high dead time

which makes the evaluation more difficult. The first measurement was made at the 20 cm geometry as the sample was hot enough. In 20 cm, 15 cm and 10 cm geometries all the measurements were made for only 1 hour for each sample where at the 0 cm geometry the measurement time was 5 hours. In 5 cm geometry the measurements were made for 3 and 5 hours. The choice was mainly for dead time consideration. Measurement for the last sample which was from the 71 MeV was made after 21 days of the irradiation. It was measured at geometry of 0 cm for 5 hours. The measurements for the monitors were made approximately between three to five months after the irradiation at geometry of 0 cm for 24 hours. This is because during this time all short lived radionuclides on the sample if present were gone and only the long lived are present. Thus the evaluation of the long live ^{65}Zn with a half-life of 244.26 days and ^{22}Na with a half-life 2.6 years from the ^{65}Cu and ^{27}Al respectively were easily possible.

4.3.7 Characteristics of the gamma-spectrometry

The spectrum evaluated at this work was complex with a large number of peaks and multiplet structure. An impression of this complexity obtained is illustrated in fig. 4.7. The number of lines is more in case of proton energy 71 MeV than 45 MeV. Also the number of produced residuals increases with the increase of energy because more reaction channels open with the increase of energy.

A restriction was adapted during the evaluation of the gamma spectra in the energy range below approximately 95 keV. The evaluation in this range is more difficult due to the fact that high-energy X-ray lines appeared in this region. A quantitative analysis of this region is not possible, because the background effect could not be defined explicitly. Also a clear allocation of the peaks to certain nuclides was not possible due to the presence of many gamma and X-ray emitting nuclides at this range.

Gamma-spectrometry of heavy nuclides becomes more difficult due to additional peaks, which are due to escape processes and gamma-gamma coincidence. Such effects falsified the activities computed from the peak areas and make wrong predictions of the presence of certain nuclides.The single and double escape peak arise in the energy of the gamma-line at 0.511 MeV and at 1.022 MeV, which is larger than the energy necessary for the production of a pair of positron-electrons. The two annihilation photons before completely absorbed in the crystal

volume, produces single escape and double escape peak in the spectrum with $E_\gamma = 511$ keV and $E_\gamma = 1022$ keV respectively. The probability of the occurrence of such effects becomes larger with rising energy. The demonstrability depends however on the size of the full energy peak and on the background.

Additional peaks caused by the coincident detection of two gamma-ray photons also appeared in the spectrum. Assume that no isomeric states are involved, the lifetime of the intermediates state is generally so short that the two gamma-rays are emitted in coincidence. It is then quite possible for both gamma-ray photons from a single decay to interact and deposit their energy within a time that is short compared with the response time of the detector. If enough of this event occurs, a sum coincidence peak will be observed in the spectrum that occurs at a pulse height corresponding to the sum of the two individual gamma-ray energies. A continuum of sum events will also occur at lower amplitudes due to the summation of partial energy loss interactions. The size of these effects and the uncertainties resulting from it is discussed in the context of the error discussion.

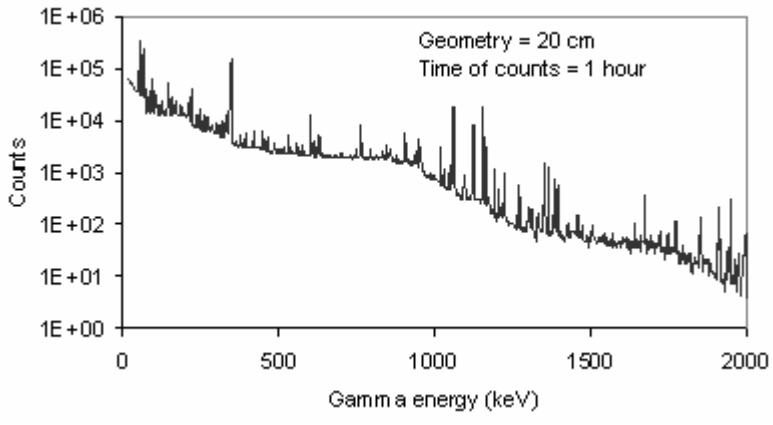

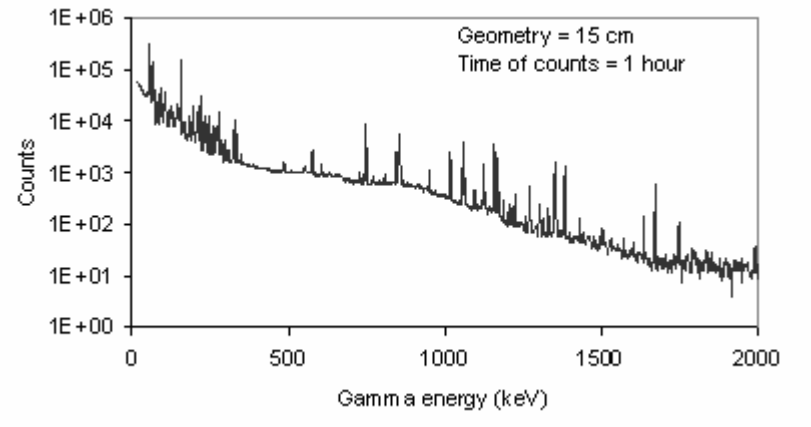

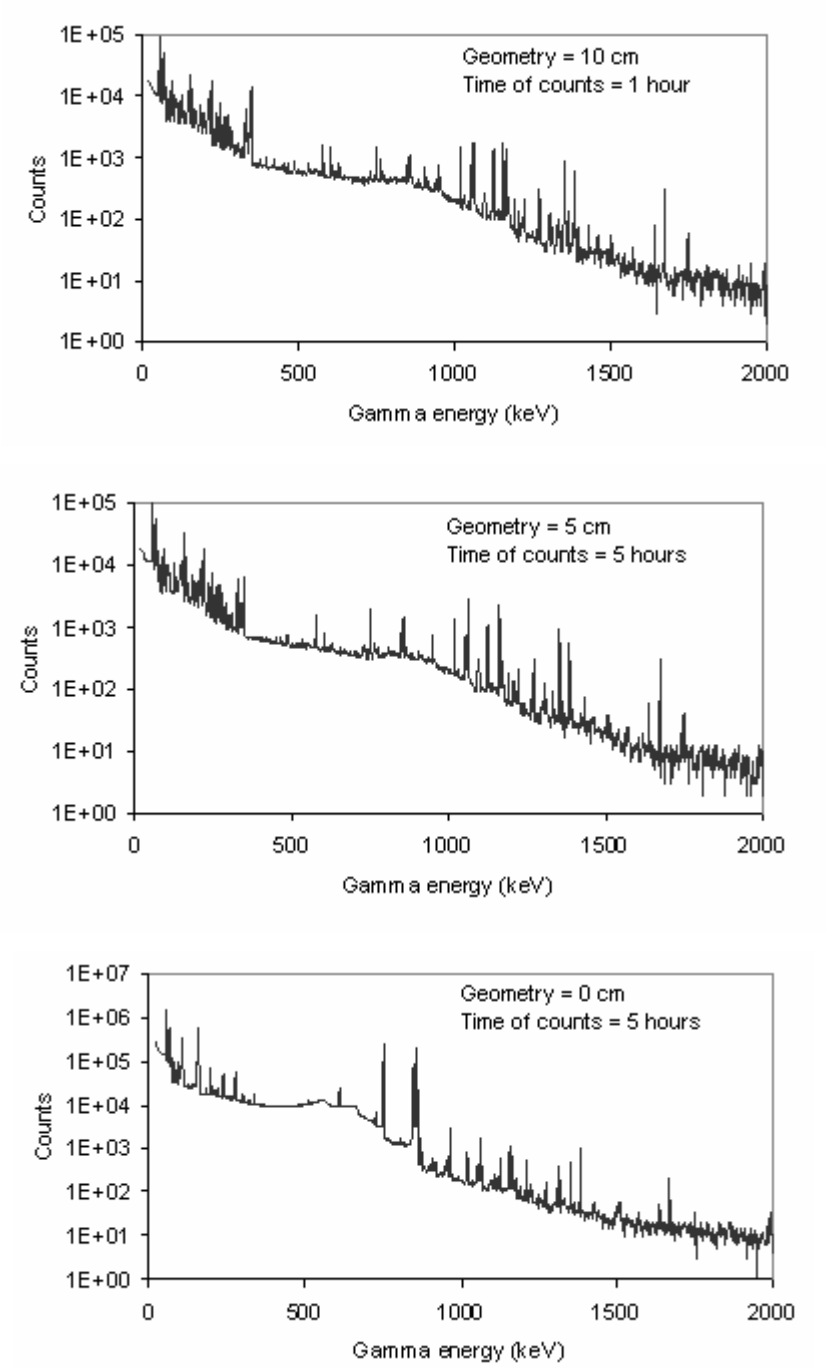

Fig. 4.7: Gamma-spectra of W targets, measured for different energies and different counting times.

4.4 Spectrum analysis

The cross-section of a nuclide is computed by equation (3.9) from the activity that is calculated by the spectrum analysis. The activity can be determined from the gamma-energy lines which are the characteristics of a nuclide. These lines appear as peaks in the spectrum. The work of

the spectrum analysis was to determine these peaks. There are different procedures for spectrum analysis according to the complexity of the spectrum. One of them is a computer program GAMMA-W by Dr. Westmeier GmbH is used in this work.

4.4.1 Evaluation with GAMMA-W

The analysis of gamma-spectra was done by the commercially available code GAMMA-W [We94], [We95]. GAMMA-W divides a spectrum gradually and independently from each other into regions. In each region the continuous background is determined and subtracted internally in such a way that the remaining impulse number and the distribution of peaks with different methods are looked for in accordance with a sensitivity given by the user and adapted in a least square fit to the spectrum. The form of a peak is Gaussian with a possible low-energy tailing. For the fit, therefore information about the full width half maxima (FWHM) and the tailing is needed. The FWHM is a function of gamma-energy and a polynomial of second degree. The appropriate coefficients of the same can be determined either by GAMMA-W or given by the user. The extent of the tailings is preset, can be given however likewise. The errors of the peak position are computed from the uncertainty of the fit parameter into the errors of the surfaces additionally those flow from the subtracted background distribution. The entire process of the spectrum analysis can take place either automatically or interactively. The interactive treatment runs off if necessary in such a way that GAMMA-W first suggests and indicates regions. This can accept by the user in accordance with its conceptions or redefine, whereby can steer this analysis within a certain framework by giving peak positions in the regions. The parameters for the description of the FWHM of the peaks and the tailing behaviour were determined from the efficiency calibration of the point sources, which were stored in a library and transferred to the analysis to find the dependence of the used detector on it. For sensitivity, a detection limit was selected according to the manual [We95]. The evaluation was accomplished over the entire channel range. Detailed tests showed that the automatic mode is not reliable enough with respect to the necessary regioning of the spectrum, peak recognition, background determination, and net peak area calculation. Thus each spectrum was measured interactively.

4.5 Determination of the flux densities of the projectiles

For calculating the cross-sections by equation (3.9) flux density of the projectiles need to be calculated. This can be done either by the direct measurements with the help of Faraday Caps or by the indirect determination from well known cross-sections of the monitor reaction. Both procedures have advantage and disadvantage. Direct measurements are possible only with high projectile energies and sufficient accuracy with high experimental expenditures. On the other hand the flux density measurement can carry out with the latter process by the help of a monitor reaction depends however on the quality of the used monitor cross-sections. Under these aspects in this work flux density calculations is done with the help of monitor reaction.

The flux densities were determined via standard monitor reaction ^{65}Cu(p,n)^{65}Zn and ^{27}Al(p,3p3n)^{22}Na. For calculating flux density, cross-section data for relevant energies from [Mi97a] were considered.

The use of aluminium and cupper as a target material has some advantages. These can be produced economically in highly pure form, so that no reactions from the impurities are required to be considered. Using the guarded Cu and Al targets in the middle the flux densities were determined by measuring the ^{65}Zn activity via the gamma-energy line at 111.5 keV and ^{22}Na activity via the gamma-energy line at 1274.5 keV. The measurements were done between 3-5 months after the irradiation. The activities were measured via the equation (3.8) and the flux density is calculated by modifying the equation (3.9) which takes the form

$$\Phi_E = \frac{A(t_{EOI})}{\sigma_E N_T (1 - e^{-\lambda t_{irr}})} = \frac{C\lambda}{I_\gamma \varepsilon_\gamma \sigma_E N_T} \cdot \frac{e^{\lambda t_d}}{(1 - e^{-\lambda t_{irr}})(1 - e^{-\lambda t_C})} \tag{4.21}$$

In fig. 4.8 cross-section for the reaction ^{65}Cu(p,n)^{65}Zn were taken from the work of Michel et al. [Mi97a]. The excitation function is composed of a maxima followed by a sharp decline which is in accordance of the theory. In fig. 4.9 cross-sections for the reaction ^{27}Al(p,3p3n)^{22}Na were considered again from Michel et al. [Mi97a]. Cross-section increases with energy after reaching a maximum then there is a plateau.

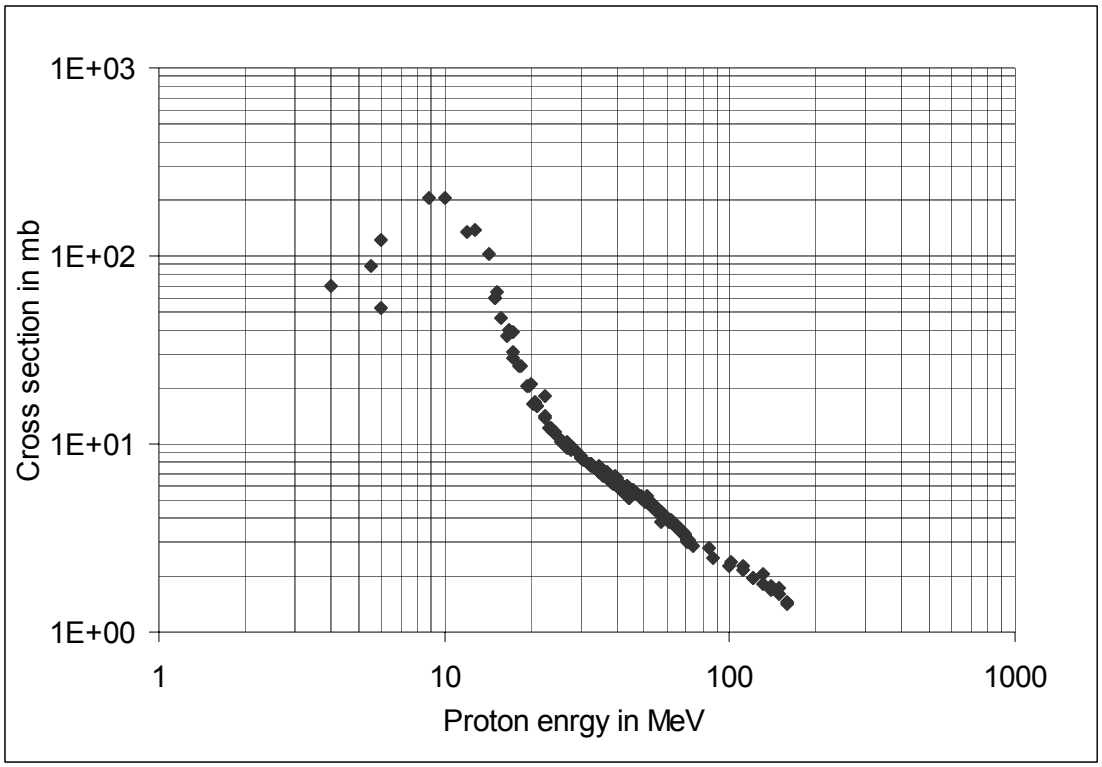

Fig. 4.8: Monitor excitation function for the reaction $^{65}Cu(p,n)^{65}Zn$ [Mi97a]

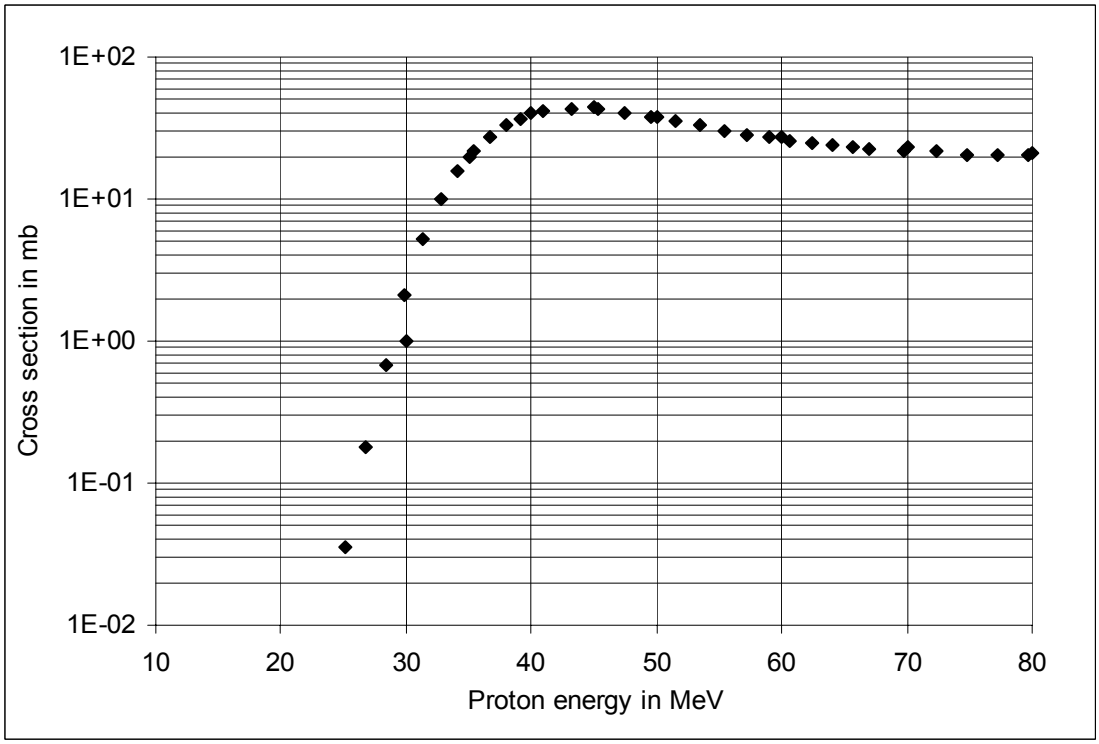

Fig. 4.9: Monitor excitation function for the reaction $^{27}Al(p,3p3n)^{22}Na$ [Mi97a]

Fig. 4.10 and 4.11 illustrate the consistency of the flux density over the different proton energies. Different measurements were taken between 3-5 months after the irradiation. From

the comparison it is clear that the flux density was constant over the whole range of the experiment. For a detailed discussion of this topic one is referred to [Mi97a].

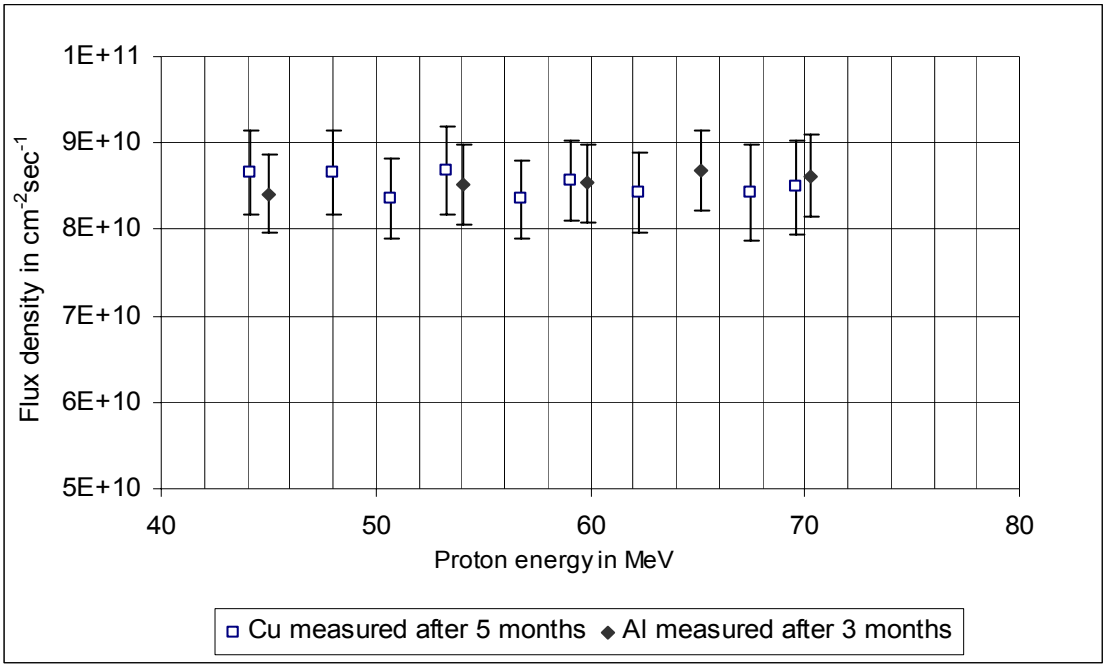

Fig.4.10: Flux density for the monitor reaction $^{65}Cu(p,n)^{65}Zn$ and $^{27}Al(p,3p3n)^{22}Na$, sample irradiated by 71 MeV proton beam.

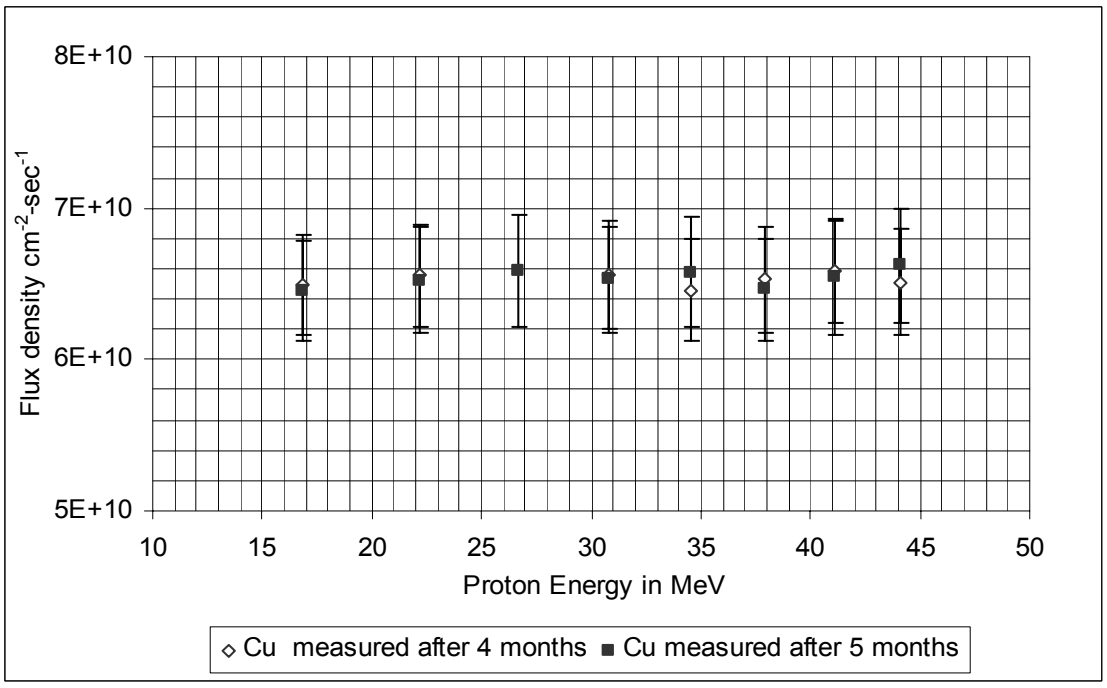

Fig. 4.11: Flux density for the monitor reaction $^{65}Cu(p,n)^{65}Zn$, sample irradiated by 45 MeV proton beam.

4.6 Identification of nuclides

The variety of the radiating nuclides produced in proton-induced reactions does not only make the determination more difficult but also the clear allocation of the peaks to certain nuclides is a tough task to perform.

All the gamma-energy lines are recorded after the evaluation of the spectrum in the output file of GAMMA-W. Then from the nuclide library all nuclides corresponding to a gamma-energy line were noted. The intensities of the lines were also noted from the nuclide library of [Ch99], [Re83] and [BN04]. In this way a Microsoft Excel ® file was made for a single measurement where in the first column the names of all the nuclides were noted and the gamma-energy measured were noted in the corresponding rows with the net peak area. In this way all the spectrums were evaluated. Then several Excel ® files were made corresponding to the different nuclides evaluated with all other information such as net peak area with their uncertainty, energy and intensity of the gamma-energy line, half-life, name of the sample, measuring date, measuring time etc. Then the activities were calculated by equation (3.8). After calculating the activity a plot was made between the activity at the begin of counting versus time of decay, which is the time that has been spanned before the specific measurement after the irradiation. Linear function available in Microsoft Excel ® of the form $y = a\exp(-\lambda x)$ was used. Here λ is the decay constant. Thus the half-life was calculated by the formula $T_{1/2} = \frac{\ln(2)}{\lambda}$. After measuring the half-life of the corresponding nuclide, it was compared with the original half-life of the nuclide. If they agrees then the identification of the corresponding nuclide is assumed to be correct. This procedure is continued for all the nuclides assumed. Half- lives those did not agree are not considered any more.

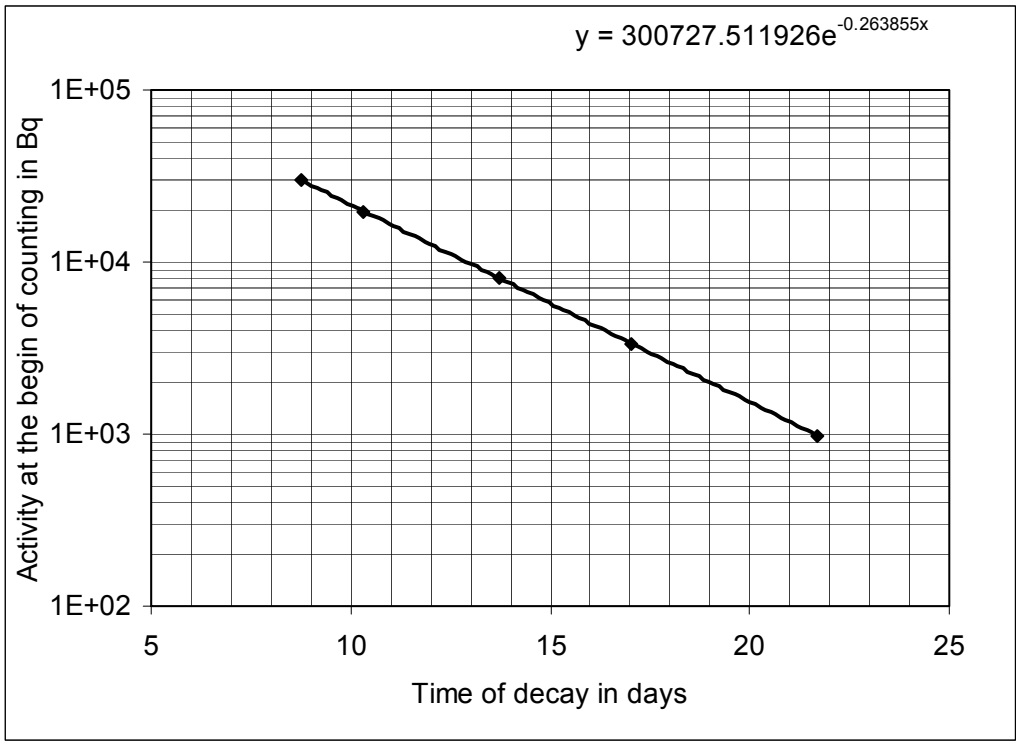

Fig. 4.12: Determination of the half-life for ^{182}Re. The calculated half-life was 63.05 days where it is 64.08 days according to [Ch99].

4.6.1 Nuclide Libraries

Nuclide libraries form the basis of the nuclide identification. In them the radioactive half-lives of the nuclides as well as the pertinent energies and their intensities stand. Three nuclide libraries were used which are [Ch99], [Re83] and [BN04]. In the case of ^{181}Re there was an inconsistency in the intensities among different libraries for gamma-energy line 360.70 keV. So the intensity supplied by [Re83] was considered as this value shows good agreement of the cross-section value with the previous work and also the branching ratios were comparatively reliable. The Q values for the reactions were taken from [Ke73].

Table 4.1: Comparison of gamma- abundances in different sources for ^{181}Re

[Ch99]		[Re83]	
E_g(keV)	Iγ	E_g(keV)	Iγ
360.70	0.20	360.70	0.12
365.57	0.56	365.50	0.56
639.30	0.064	639.09	0.064

4.7 Analysis of uncertainty

Every scientific work should be presented accompanied with its accountability. Recently this is indicated as uncertainty which was previously treated as error. The word uncertainty means doubt and uncertainty of measurement means doubt about the validity of the result of a measurement. In general the result of a measurement is only an estimate of the value of the measurand and thus is complete only when accompanied by the statement of the uncertainty of that estimation. For the results obtained here two types of uncertainty would be considered; those in the proton energy in the target and those of the cross-section.

Consider a measurand *Y*, which is not determined directly but has to be determined by *N* other quantities $X_1, X_2, ...X_N$ through a functional relationship *f*,

$$Y = f(X_1, X_2, ...X_N) \tag{4.21}$$

The input quantities $X_1, X_2, ...X_N$ upon which the output quantity *Y* depends, may themselves be viewed as measurand and depend on other quantities, including corrections and correction factors for systematic effects.

An estimate of the measurand *Y*, denoted by *y*, is obtained from equation (4.21) using input estimates $x_1, x_2, ...x_N$ for the values of the *N* quantities $X_1, X_2, ...X_N$. Thus the output estimate *y*, which is the result of the measurement, is given by

$$y = f(x_1, x_2, ...x_n) \tag{4.22}$$

The combined standard uncertainty of the estimate *y* is denoted by $u_c(y)$ and is obtained by

$$u_c^2(y) = \sum_{i=1}^{n} \left(\frac{\partial f}{\partial x_i} \right)^2 u^2(x_i) \tag{4.24}$$

The combined variance $u_c^2(y)$ can be viewed as a sum of terms, each of which represents the estimated variance associated with the output estimate *y* generated by the estimated variance x_i. Thus equation (4.24) can be written as

$$u_c^2(y) = \sum_{i=1}^{N} \left[c_i u(u(x_{i)} \right]^2 = \sum_{i=1}^{N} u_i^2(y) \tag{4.25}$$

Where

$$c_i \equiv \frac{\partial f}{\partial x_i}, \quad u_i(y) \equiv |c_i| u(x_i) \tag{4.26}$$

For more detail description on uncertainty measurement one is referred to [Bi95].

4.7.1 Uncertainties of proton energies

There are three sources of uncertainties in the proton energy in a target.

1. The uncertainty ΔE_A associated with the energy of the protons leaving the accelerator.

2. The proton energy is declined from initial energy $E_{n,i}$ to a final energy $E_{n,f}$ due to the slowing down process by the interaction with the target. This results into an energy spread with a half width $\Delta E_{loss} = (E_{n,i} - E_{n,f})$

3. The statistical nature of the slowing down process accompanied with an energy straggling that can be described according to [Bo15] by Gaussian distribution with a width straggling parameter α_i.

Consequently, the uncertainty of proton energy E_n in the nth target foil of a stack is given by

$$\Delta E_n = \sqrt{\Delta E^2 + \Delta E_{loss}^2 + \left(\sum_{i=1}^{n} \alpha_i^2 \right)} \tag{4.22}$$

Generally it is observed that, these resulted uncertainties are less than 5% in all targets.

4.7.2 Uncertainties of cross-sections

Uncertainty in the determination of net peak area:
The uncertainty associated with each net peak areas during the evaluation of the spectrum was determined by the GAMMA-W. This is another advantage of this program that the net peak areas counted are associated with their respective uncertainties. The Poisson uncertainties of the counts in the individual channels and the uncertainty of the background determination according to the law of error propagation through the unfolding procedure are considered here. If a peak is produced by different nuclides, it is difficult to assign for a particular nuclide. If the contributions were not negligible and the activity of one contributing nuclides can be determined using another line or in a later spectrum, the interfering lines can be corrected using this activity. If the contributions of other nuclides to a peak are very small no correction need to be applied. Due to this procedure it is assumed to have a maximum inaccuracy of 5% due to contributions of other nuclides. In average this uncertainty was always tried to keep smaller.

Uncertainty of half-lives
The half-lives of the corresponding nuclides considered here were taken from [Ch99]. This is a reliable source of nuclear data. There is no large deviation of half-lives in compared with other sources such as [BN04] and [Re83] which are the other reliable sources for nuclear data. Typically an uncertainty of 1% for this quantity was assumed. Larger uncertainties if present would have shown up during the half-life control procedure.

Uncertainty of gamma-abundances
Gamma-abundances were also taken from [Ch99]. There were almost no inconsistencies between the different sources except for $^{181}\mathrm{Re}$. In this case the branching ratios between different gamma-energy lines seemed to be not reliable while the values taken from [Re83] show consistency with different gamma-energy lines of $^{181}\mathrm{Re}$. Normally the strongest gamma-energy lines were considered for each element. An average of 2% uncertainty was considered for this effect.

Uncertainty of detector efficiency

The calibration standards used for this work were certified by Physikalisch-Technische Bundesanstalt (PTB) at Braunschweig, and have a certified uncertainty of $\leq 2\%$. The detector's efficiencies were measured in different geometries associated with a total uncertainty of the full energy peak efficiency of $\approx 5\%$.

Uncertainty of mass of the irradiated nuclei

Each foil was weighted with an absolute uncertainty of 2 mg.

Uncertainty of flux density

The flux densities were determined via monitor reaction $^{65}Cu(p,n)^{65}Zn$ and $^{27}Al(p,3p3n)^{22}Na$ by using cross-sections given in [Mi97a]. Methods are described in [Bu95] and [Mi97b]. The uncertainty of the flux density is lead by the uncertainties of efficiency and the mass of the monitor foil which is summed up to 5%. No uncertainties were attributed to the monitor cross-sections due to an uncertainty of the proton energy because the monitor excitation functions do not vary in the region covered.

Uncertainty of irradiation time, decay time and counting time

The uncertainty concerning the time scale was considered as negligible.

Uncertainties of impurities

The high purity of the target foil allows neglecting the contributions of other constituents.

Gamma-gamma coincidence

At very small distance this effect plays a role. Most of the measurements were done in more than 5 cm. Even in 0 cm this effect was not visible. Thus this effect was taken as a general uncertainty due to gamma-gamma coincidence in the case of coincident gamma-rays.

Constancy of flux density over irradiation time

The beam intensities were continuously monitored and recorded. The uncertainties due to fluctuations in the beam intensities were negligible. Moreover they affect only for the cross-sections for very short-lived nuclides that was not considered in this case.

Dead time and pile-up losses in gamma-spectroscopy

The dead time of the detector was automatically corrected. Pile-up were not seen because the distance between the sample and the detector were varied in the way that the counting rates were low enough to avoid both pile-up and failure of automatic dead time correction.

Recoil losses and recoil contaminations

By measuring the inner foils in a mini-stack only, both recoil losses and recoil contamination was neglected.

Chapter 5

5.1 Experimental results

The experimental results are discussed in this chapter. Altogether 67 cross-sections were determined for residual nuclide production in 4 proton-induced reactions with target element tungsten in the energy region between 10 to 70 MeV. Radioactive nuclides with half-lives between 20 hours to 38 days were identified. The magnitude of the cross-sections ranged from 1.98 E+01 to 5.38 E+02 mb.

The different reactions obtained are

$^{nat}W(p,xn)^{181}Re$ the half-life of ^{181}Re is $T_{1/2} = 19.9$ h

$^{nat}W(p,xn)^{182}Re$ the half-life of ^{182}Re is $T_{1/2} = 64.08$ h

$^{nat}W(p,xn)^{184}Re$ the half-life of ^{184}Re is $T_{1/2} = 38$ d

$^{nat}W(p,2pxn)^{177}Ta$ the half-life of ^{177}Ta is $T_{1/2} = 56.56$ h

Cross-sections for a nuclide were calculated for different gamma-energy lines in order to ensure the reliability of the work. The results were in good agreement with each other which proves the consistency of the obtained results. The experimentally obtained results were compared with other previous work of Ullah [Ul04], Protoschill [Pr97a] and with different theoretical codes. The comparison with previous experimental work is discussed in this chapter while with the codes in the following chapter.

The activities and the cross-sections were calculated according to the equation (3.8) and (3.9) respectively. The activity depends on the time of irradiation by equation (3.6) which shows activity is an exponential function of time.

5.2 Earlier work of other authors

The experimentally obtained results were compared with some other previous works. There were not much data available for comparison. However for the excitation function $^{nat}W(p,xn)^{184}Re$, the comparison was done with the work of Ullah [Ul04]. The energy range was between 10-45 MeV. There was no other data available for this reaction. For

^{nat}W(p,xn)^{182}Re comparison was done with the work of Ullah [Ul04] and Protoschill [Pr97a]. Ullah's data were again for 10-45 MeV and Protoschill's work was in the energy range between 65 MeV to 1.2 GeV. The results for ^{nat}W(p,xn)^{181}Re were compared with the work of Protoschill. The data ranged from 65 MeV to 1.2 GeV. For ^{nat}W(p,2pxn)^{177}Ta there was no previous work available to compare.

5.3.1 Results for ^{184}Re

The half-life of ^{184}Re was calculated from the plot of activity at the begin of counting versus time of decay. The measured half-life of ^{184}Re was 38.9 days shown in fig 5.1, where the half-life obtained from [Ch99] was 38 days. Thus the identification of the nuclide was considered as correct.

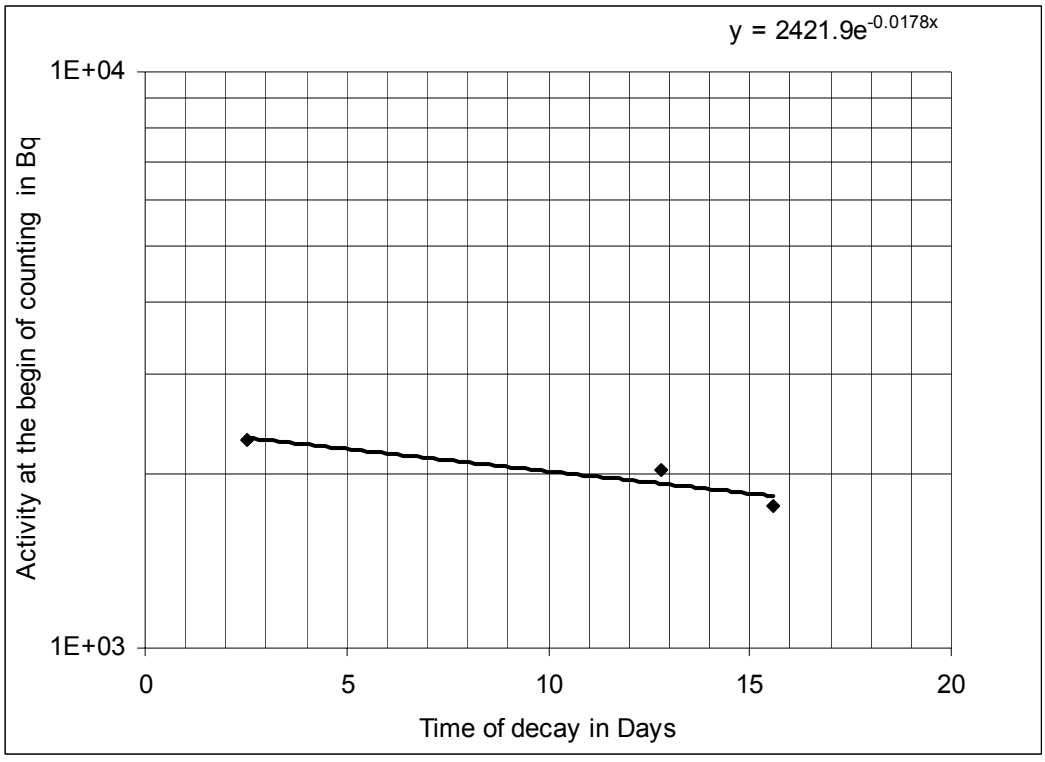

Fig.5.1: Determination of the half-life for ^{184}Re.

For ^{184}Re, measurements were made for the gamma-energy line 903.3 keV, 894.9 keV and 792.07 keV with gamma-abundances 0.379, 0.156 and 0.375 respectively.

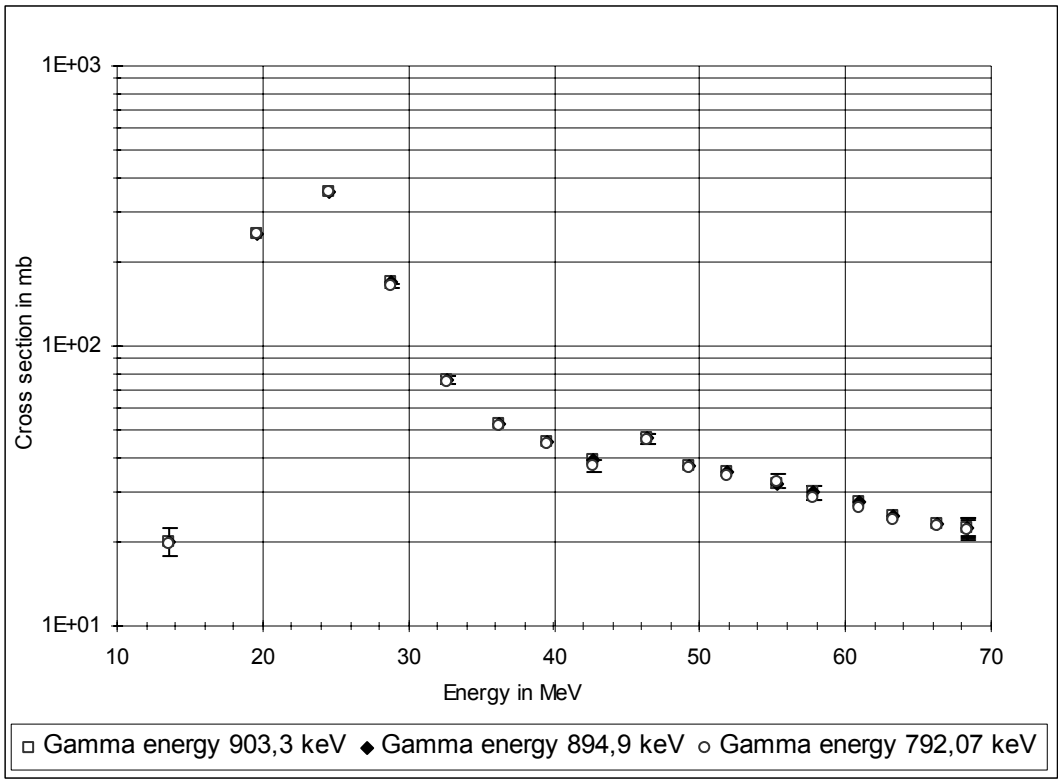

Fig.5.2: Excitation function for different gamma-energy lines of the reaction $^{nat}W(p,xn)^{184}Re$ with associated uncertainties

In fig 5.2, it is evident that the excitation functions for different gamma-energy lines are in good agreement with each other. This proves the consistency of the measurement. Also it is clear that the associated uncertainty is small. The excitation function increases with the increase of proton energy and has a resonance at 24.52 MeV. Then there is a gradual decrease. From 46 MeV to the end this decrease is almost linear. This decrease corresponds to pre-equilibrium reaction. There is a little fluctuation of the data at 46 MeV. This data corresponds to the sample number 9 irradiated by 71 MeV proton beam. This was measured alone after the total measurement and it was measured only once. The presence of secondary neutron or the attenuation of flux density may also another cause for this fluctuation.

Table 5.1: Cross-section data for the reaction $^{nat}W(p,xn)^{184}Re$ at $E_\gamma = 894.9$ keV with $I_\gamma = 0.156$

Target	Reaction	Product	$E_p$in MeV	u(E_p) in MeV	σ in mb	u(σ) in mb
^{nat}W	p,xn	^{184}Re	68.42	4.00E-01	2.25E+01	1.99E+00
^{nat}W	p,xn	^{184}Re	66.27	4.73E-01	2.27E+01	1.72E+00
^{nat}W	p,xn	^{184}Re	63.27	5.46E-01	2.41E+01	1.84E+00
^{nat}W	p,xn	^{184}Re	60.98	5.90E-01	2.64E+01	2.17E+00
^{nat}W	p,xn	^{184}Re	57.79	6.51E-01	2.87E+01	2.29E+00
^{nat}W	p,xn	^{184}Re	55.34	6.93E-01	3.29E+01	2.65E+00
^{nat}W	p,xn	^{184}Re	51.88	7.45E-01	3.45E+01	2.70E+00
^{nat}W	p,xn	^{184}Re	49.20	7.85E-01	3.65E+01	2.79E+00
^{nat}W	p,xn	^{184}Re	46.42	8.25E-01	4.64E+01	3.64E+00
^{nat}W	p,xn	^{184}Re	42.64	4.65E-01	3.71E+01	2.77E+00
^{nat}W	p,xn	^{184}Re	39.54	5.59E-01	4.46E+01	3.30E+00
^{nat}W	p,xn	^{184}Re	36.23	6.37E-01	5.16E+01	3.85E+00
^{nat}W	p,xn	^{184}Re	32.68	7.12E-01	7.39E+01	5.45E+00
^{nat}W	p,xn	^{184}Re	28.83	7.89E-01	1.64E+02	1.21E+01
^{nat}W	p,xn	^{184}Re	24.52	8.77E-01	3.54E+02	2.59E+01
^{nat}W	p,xn	^{184}Re	19.62	9.91E-01	2.51E+02	1.84E+01
^{nat}W	p,xn	^{184}Re	13.54	1.18E+00	1.98E+01	1.47E+00

5.3.2 Results for ^{182}Re

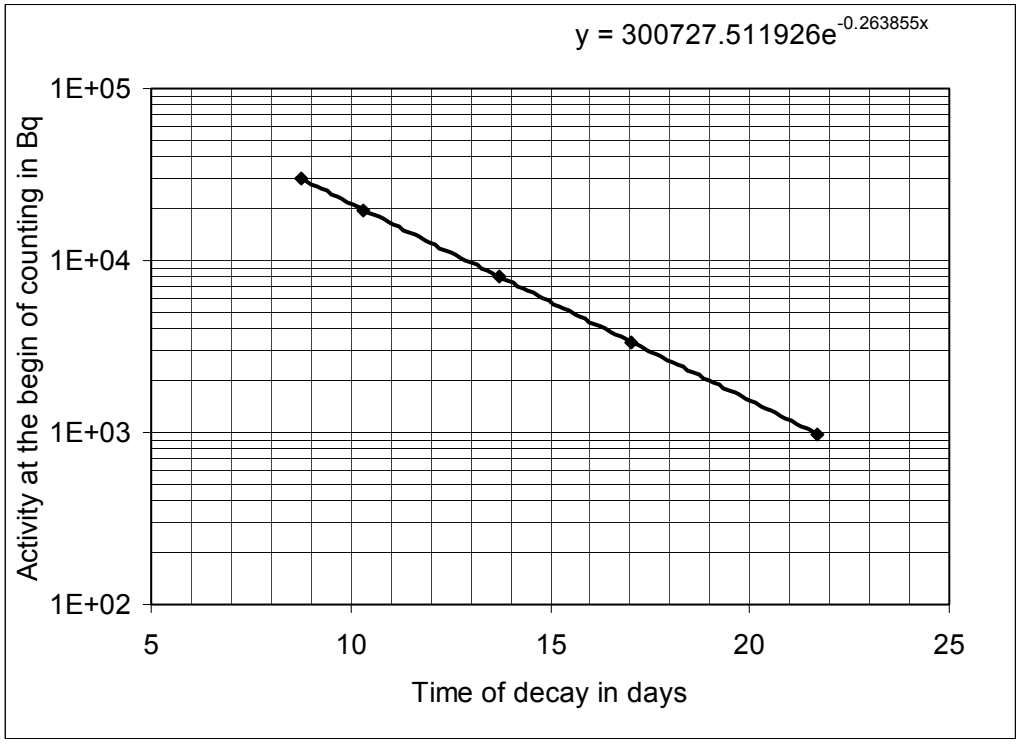

Fig.5.3: Determination of the half-life for ^{182}Re .

The measured half-life of ^{182}Re was 63.05 days shown in fig.5.3, where the half-life obtained from [Ch99] was 64.08 days. Thus it can be said that the identification of the nuclide was correct

For ^{182}Re, measurements were made for the gamma-energy line 1221.4 keV, 1121.3 keV and 229.3 keV with gamma-abundance 0.174, 0.22 and 0.26 respectively.

The excitation functions obtained for different gamma-energy lines are in good agreement with each other which is evident from the fig 5.4. The excitation function has two apparent maxima followed by a plateau.

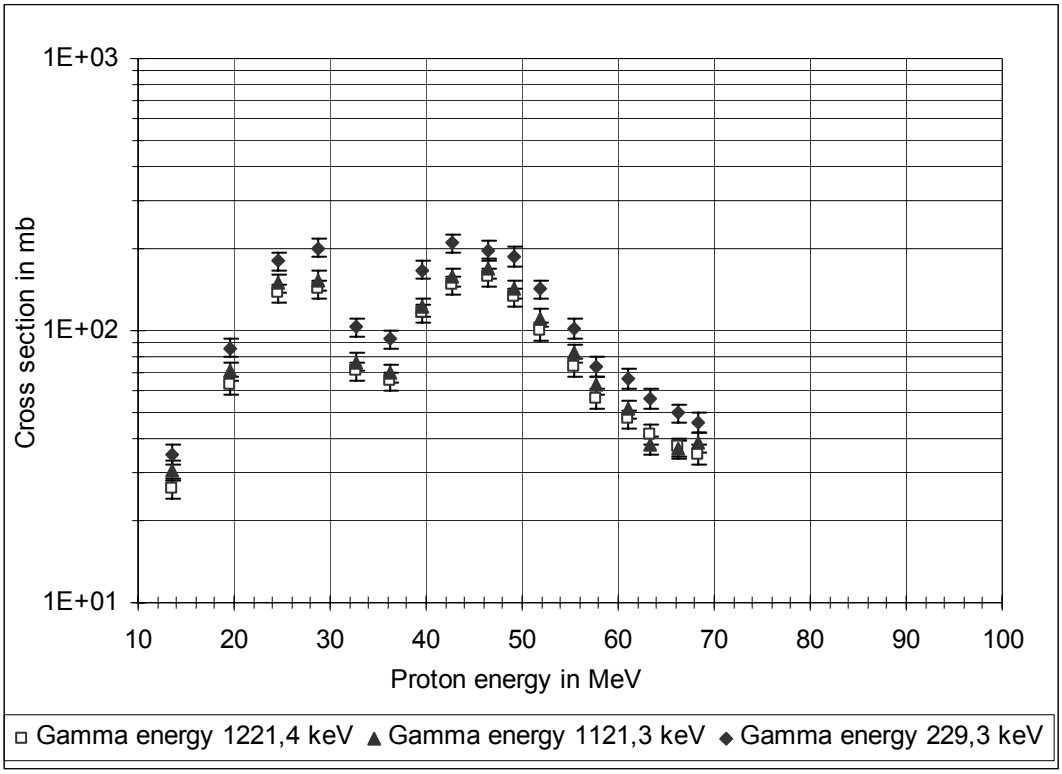

Fig.5.4: Excitation function for different gamma-energy lines of the reaction ^{nat}W(p,xn)^{182}Re with associated uncertainties.

Table 5.2: Cross-section data for the reaction $^{nat}W(p,xn)^{182}Re$ at E_γ = 1221.4 keV with I_γ = 0.174.

Target	Reaction	Product	E_p in MeV	u(Ep) in MeV	σ in mb	u(σ) in mb
^{nat}W	p,xn	^{182}Re	68.42	4.00E-01	3.91E+01	3.18E+00
^{nat}W	p,xn	^{182}Re	66.27	4.73E-01	3.67E+01	2.87E+00
^{nat}W	p,xn	^{1182}Re	63.27	5.46E-01	3.80E+01	3.02E+00
^{nat}W	p,xn	^{182}Re	60.98	5.90E-01	5.16E+01	4.02E+00
^{nat}W	p,xn	^{1182}Re	57.79	6.51E-01	6.33E+01	4.98E+00
^{nat}W	p,xn	^{182}Re	55.34	6.93E-01	8.23E+01	6.68E+00
^{nat}W	p,xn	^{182}Re	51.88	7.45E-01	1.11E+02	8.84E+00
^{nat}W	p,xn	^{182}Re	49.20	7.85E-01	1.42E+02	1.10E+01
^{nat}W	p,xn	^{1182}Re	46.42	8.25E-01	1.70E+02	1.36E+01
^{nat}W	p,xn	^{182}Re	42.64	4.65E-01	1.57E+02	1.18E+01
^{nat}W	p,xn	^{182}Re	39.54	5.59E-01	1.22E+02	9.19E+00
^{nat}W	p,xn	^{182}Re	36.23	6.37E-01	7.00E+01	5.38E+00
^{nat}W	p,xn	^{182}Re	32.68	7.12E-01	7.68E+01	5.90E+00
^{nat}W	p,xn	^{182}Re	28.83	7.89E-01	1.53E+02	1.18E+01
^{nat}W	p,xn	^{182}Re	24.52	8.77E-01	1.50E+02	1.13E+01
^{nat}W	p,xn	^{182}Re	19.62	9.91E-01	7.13E+01	5.44E+00
^{nat}W	p,xn	^{182}Re	13.54	1.18E+00	3.06E+01	2.41E+00

5.3.3 Results for ^{181}Re

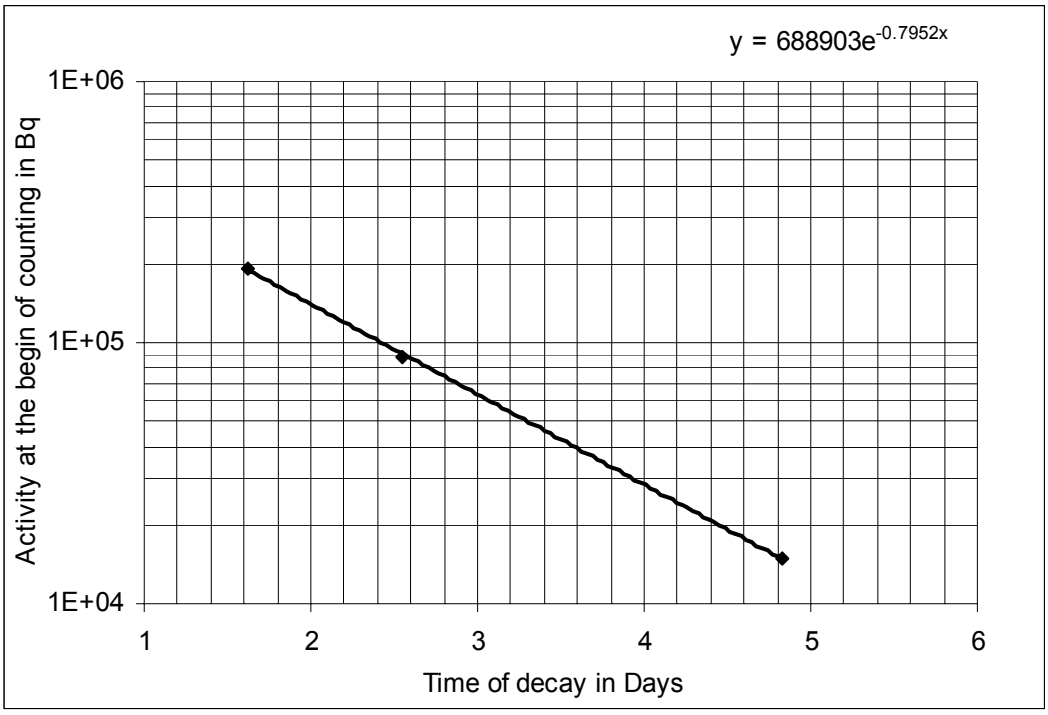

Fig.5.5: Determination of the half-life for ^{181}Re.

The measured half-life of ^{181}Re was 20.9 days shown in fig 5.5 where the half-life obtained from [Re83] was 20 days which confirms the identification of the nuclide.

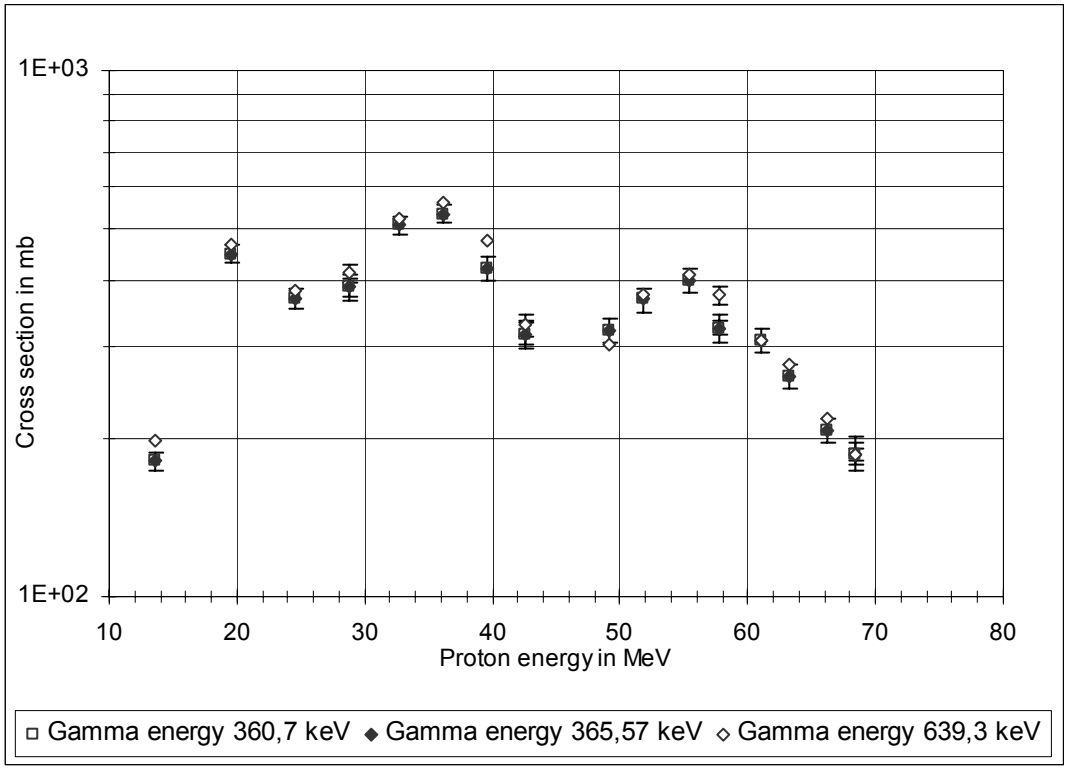

Fig.5.6: Excitation function for different gamma-energy lines of the reaction ^{nat}W(p,xn)^{181}Re with associated uncertainties.

Table 5.3: Cross-section data for the reaction ^{nat}W(p,xn)^{181}Re at E_γ = 365.57 keV with I_γ = 0.56 [Re83].

Target	Reaction	Product	E_p in MeV	u(Ep) in MeV	σ in mb	u(σ) in mb
^{nat}W	p,xn	^{181}Re	68.42	4.00E-01	1.88E+02	5.28E+00
^{nat}W	p,xn	^{181}Re	66.27	4.73E-01	2.08E+02	1.07E+01
^{nat}W	p,xn	^{181}Re	63.27	5.46E-01	2.64E+02	1.35E+01
^{nat}W	p,xn	^{181}Re	60.98	5.90E-01	3.09E+02	1.59E+01
^{nat}W	p,xn	^{181}Re	57.79	6.51E-01	3.26E+02	1.91E+01
^{nat}W	p,xn	^{181}Re	55.34	6.93E-01	4.01E+02	2.07E+01
^{nat}W	p,xn	^{181}Re	51.88	7.45E-01	3.70E+02	1.94E+01
^{nat}W	p,xn	^{181}Re	49.20	7.85E-01	3.23E+02	1.68E+01
^{nat}W	p,xn	^{181}Re	42.64	4.65E-01	3.18E+02	1.60E+01
^{nat}W	p,xn	^{181}Re	39.54	5.59E-01	4.24E+02	2.19E+01
^{nat}W	p,xn	^{181}Re	36.23	6.37E-01	5.38E+02	2.14E+01
^{nat}W	p,xn	^{181}Re	32.68	7.12E-01	5.11E+02	2.02E+01
^{nat}W	p,xn	^{181}Re	28.83	7.89E-01	3.91E+02	1.52E+01
^{nat}W	p,xn	^{181}Re	24.52	8.77E-01	3.70E+02	1.64E+01
^{nat}W	p,xn	^{181}Re	19.62	9.91E-01	4.51E+02	1.75E+01
^{nat}W	p,xn	^{181}Re	13.54	1.18E+00	1.82E+02	7.26E+00

For ^{181}Re, measurements were made for the gamma-energy line 639.3 keV, 365.57 keV and 360.3 keV with gamma-abundance 0.64, 0.56 and 0.12 respectively

There is a little discrepancy in the excitation function ^{nat}W(p,xn)^{181}Re measured for different gamma-energy lines. This can be attributed to the inconsistency of the gamma-abundance from different sources. For the gamma-energy 360 keV in [Ch99] it was 20, while in [Re83] it was 12. In [BN04] there was no information for this particular gamma-energy line. For the other two energy line the values were in accordance. The excitation function has three maxima at 19.62 MeV, 36.23 MeV and 55.34 MeV then decreased monotonously.

5.3.4 Results for ^{177}Ta

The measured half-life of ^{177}Ta was 57.3 days shown in fig.5.7 where the half-life obtained from [Ch99] was 56.56 days. Thus the identification of the nuclide was assumed to be correct.

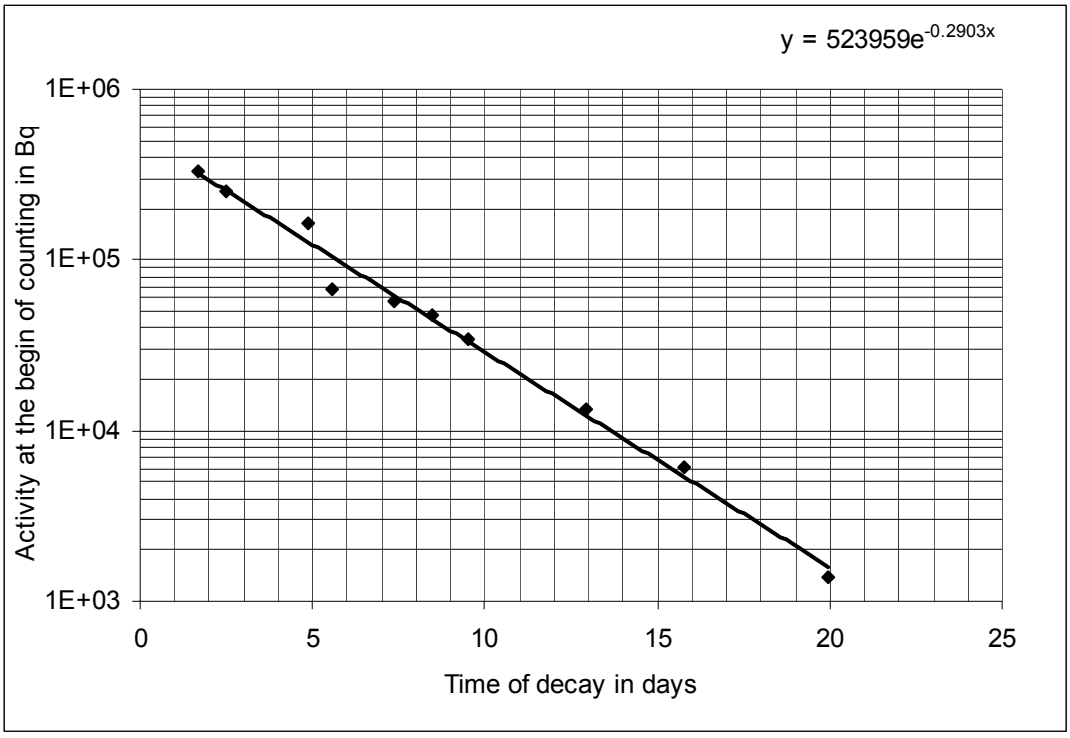

Fig.5.7: Determination of the half-life for ^{177}Ta

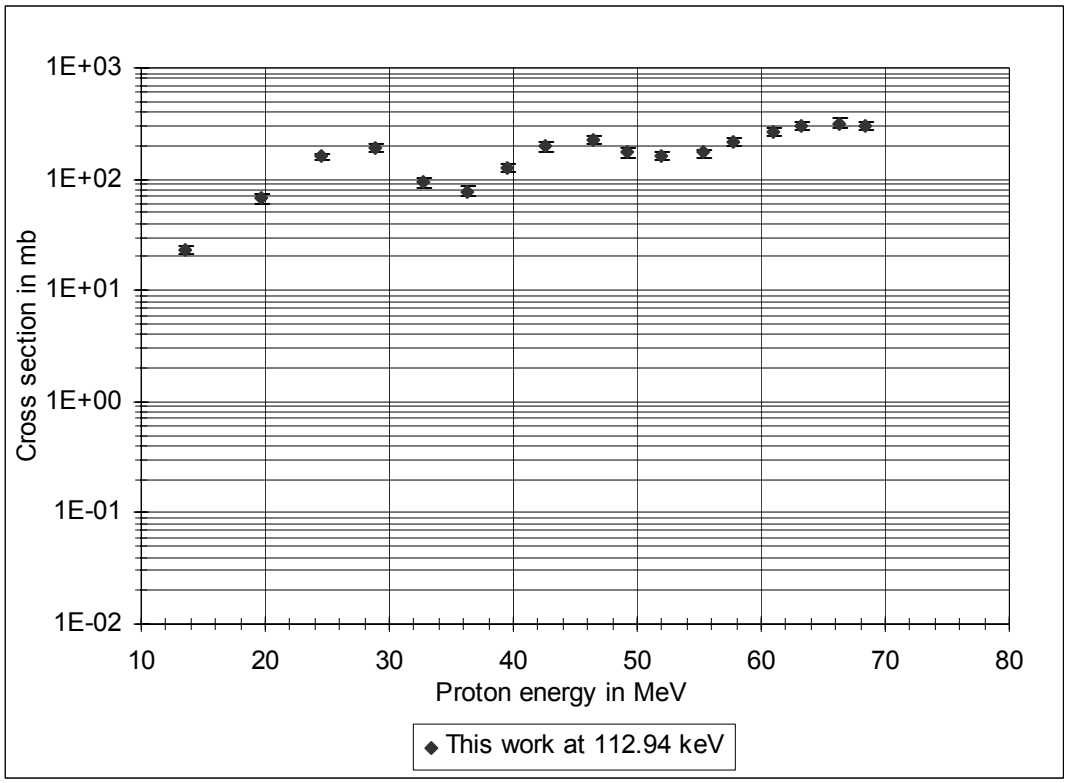

Fig.5.8: Excitation function for the reaction $^{nat}W(p,2pxn)^{177}Ta$ at E_γ = 112.94 keV with I_γ = 0.072.

Table 5.4: Cross-sections data for the reaction $^{nat}W(p,2pxn)^{177}Ta$ at E_γ = 112.94 keV with I_γ = 0.072 [Ch99].

Target	Reaction	Product	E_p in MeV	u(Ep) in MeV	σ in mb	u(σ) in mb
^{nat}W	p,2pxn	^{177}Ta	68.42	4.00E-01	3.03E+02	2.39E+01
^{nat}W	p,2pxn	^{177}Ta	66.27	4.73E-01	3.19E+02	2.96E+01
^{nat}W	p,2pxn	^{177}Ta	63.27	5.46E-01	2.97E+02	2.40E+01
^{nat}W	p,2pxn	^{177}Ta	60.98	5.90E-01	2.71E+02	2.14E+01
^{nat}W	p,2pxn	^{177}Ta	57.79	6.51E-01	2.16E+02	1.73E+01
^{nat}W	p,2pxn	^{177}Ta	55.34	6.93E-01	1.72E+02	1.40E+01
^{nat}W	p,2pxn	^{177}Ta	51.88	7.45E-01	1.63E+02	1.36E+01
^{nat}W	p,2pxn	^{177}Ta	49.20	7.85E-01	1.73E+02	1.54E+01
^{nat}W	p,2pxn	^{177}Ta	46.42	8.25E-01	2.29E+02	1.75E+01
^{nat}W	p,2pxn	^{177}Ta	42.64	4.65E-01	1.95E+02	1.69E+01
^{nat}W	p,2pxn	^{177}Ta	39.54	5.59E-01	1.26E+02	1.17E+01
^{nat}W	p,2pxn	^{177}Ta	36.23	6.37E-01	7.76E+01	7.83E+00
^{nat}W	p,2pxn	^{177}Ta	32.68	7.12E-01	9.28E+01	8.59E+00
^{nat}W	p,2pxn	^{177}Ta	28.83	7.89E-01	1.91E+02	1.67E+01
^{nat}W	p,2pxn	^{177}Ta	24.52	8.77E-01	1.60E+02	9.00E+00
^{nat}W	p,2pxn	^{177}Ta	19.62	9.91E-01	6.76E+01	7.11E+00
^{nat}W	p,2pxn	^{177}Ta	13.54	1.18E+00	2.32E+01	2.23E+00

For ^{177}Ta measurements was made for the gamma-energy line 112.94 keV with gamma abundance 0.072. The only other gamma-energy line that ^{177}Ta poses is at 208 keV but it has a very low gamma-abundance which was not able to detect.

It is evident from fig. 5.8 that the excitation function for ^{177}Ta is composed of a three step process. The excitation function has three maxima at 28.83 MeV, 46.42 MeV, and 51.88 MeV followed by a decline which is not evident here.

5.4. Comparisons

Comparison was done with the previous work of Ullah [Ul04] and Protoschill [Pr97a].

5.4.1 Comparison for the excitation function ^{nat}W(p,xn)^{184}Re

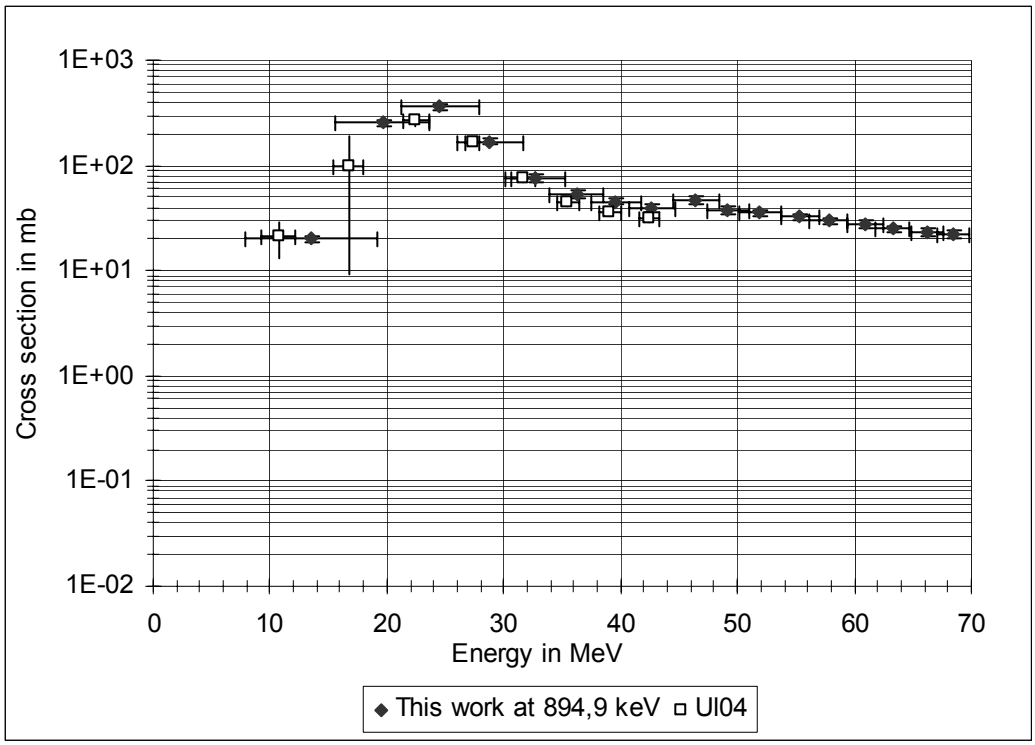

Fig.5.9: Comparison of the experimentally obtained data for the reaction ^{nat}W(p,xn)^{184}Re with other experimental work

For comparison Uallah's [Ul04] work was considered. The energy range was between 10 to 45 MeV. A little discrepancy is observed.

5.4.2 Comparison for the excitation function $^{nat}W(p,xn)^{182}Re$

For comparison Uallah's [Ul04] and Protoschill's work were considered. Ullah's work was in the energy range between 10 to 45 MeV while Protoschill worked at high energy range i.e. 68 MeV to 1.2 GeV. The obtained results were in very good agreement with each other in all energy range.

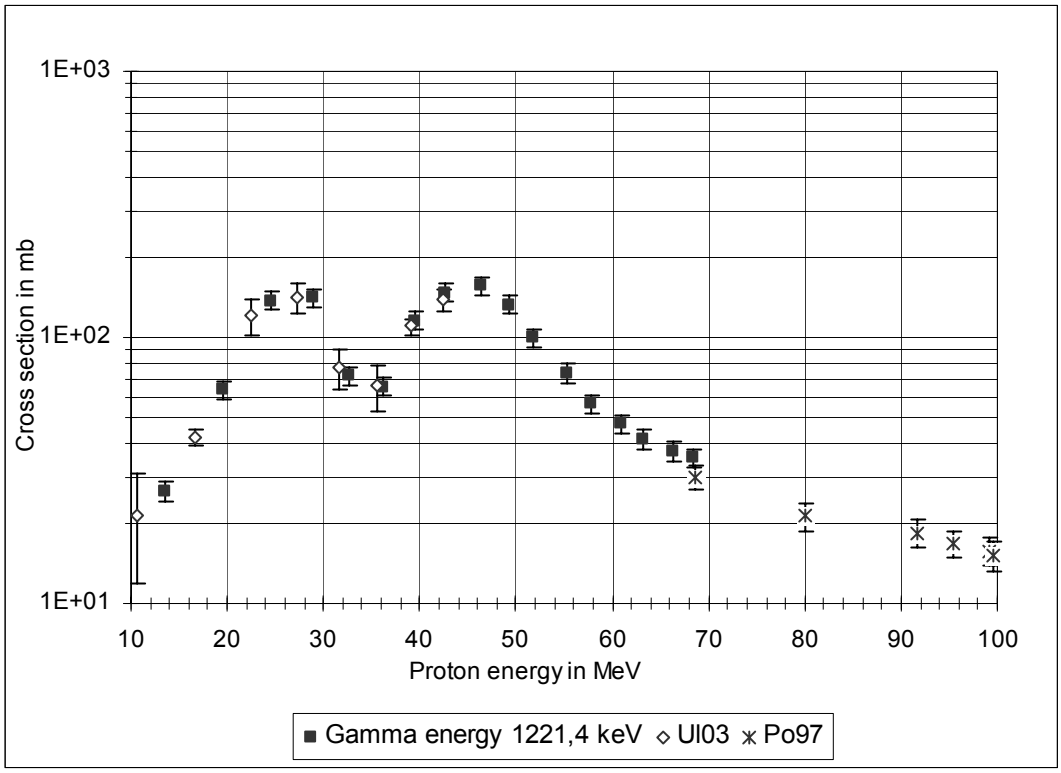

Fig.5.10: Comparison of the experimentally obtained data for the reaction $^{nat}W(p,xn)^{182}Re$ with other experimental work. The uncertainties of the proton energies are removed for a better view.

5.4.3 Comparison for the excitation function $^{nat}W(p,xn)^{181}Re$

The experimentally obtained data were compared with Protoschill's [Pr97a] work. It was in the energy region from 68 MeV. At 68 MeV the data of this work is higher than that of Protoschill by a factor 1. This may be attributed due to the discrepancy in the intensity in different sources.

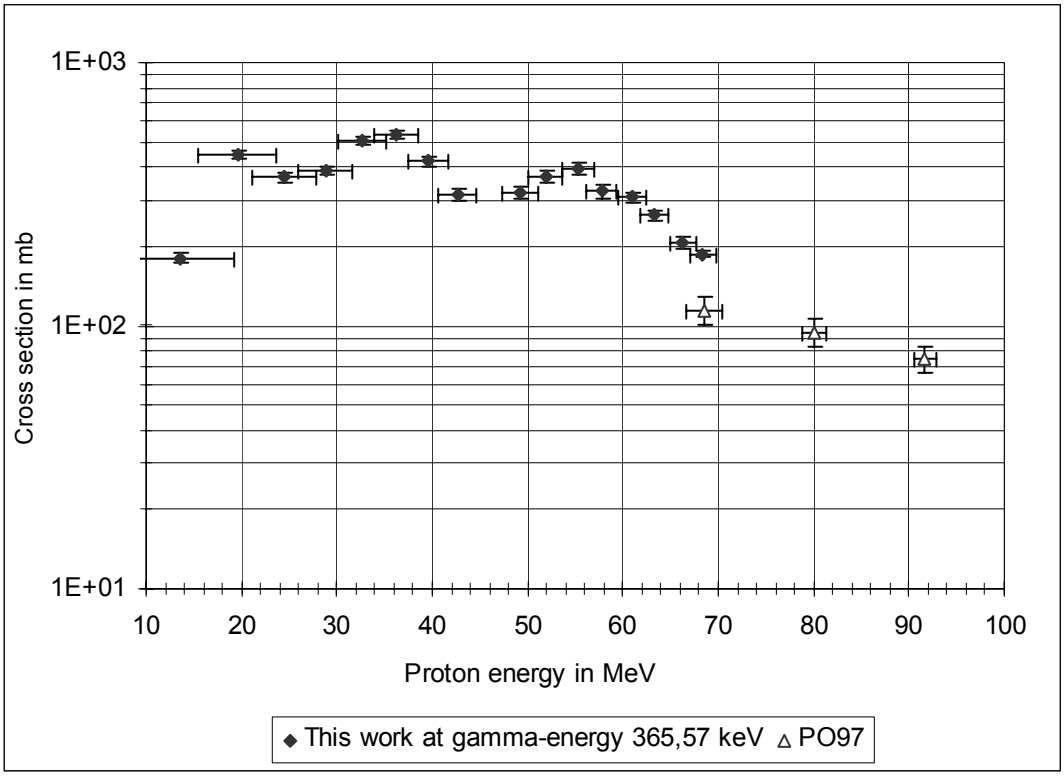

Fig.5.11: Comparison of the experimentally obtained data for the reaction $^{nat}W(p,xn)^{181}Re$ with other experimental work

5.4.4 Comparison for the excitation function $^{nat}W(p,2pxn)^{177}Ta$

There was no data available to compare.

Chapter 6

6.1 Models for nuclear reaction

A model gives us complete understanding of a physical process. It allows extrapolation and prediction of experimental data. In nuclear physics it is convenient to formulate such models in order to describe reaction mechanism.

There are several models to formulate the nuclear reactions. In direct reaction model single interaction between the projectile and one or several nucleons of the target nucleus is treated. In compound nucleus model it is assumed that the projectile is captured by the target nucleus resulting to the compound nucleus. The captured particle then shared its energy with all the nucleons in the target nucleus and the target nucleus attains statistical equilibrium. Thus the decay of the compound nucleus is described by the equilibrium statistical mechanics.

These models were successful in many situations. But in some cases where continuous high energy components were observed that are not consistent with the prediction of these models. These phenomenons have been treated by classical models called pre-equilibrium model. These models are capable of reproducing the shapes and absolute cross-section of the spectra. Some of the models that formulate the TALYS and AREL code which are used for comparison of the experimental results of this work are described in this chapter.

6.1.1 Exciton model

Griffin formulated a model [Gr66], [Gr67], [Gr68] in which it was assumed that equilibration between target and projectile is achieved by a succession of two body interactions. Each state is characterized by a number of excited particles (p) plus holes (h) or excitons ($n=p+h$) defined with respect to the Fermi energy of the target. For each exciton number, some fractions of states have particles that are unbound. It was assumed that every partition of energy for a given exciton number occurred with a priori probability during the equilibration process. He further assumed a predominance of transitions to more complicated states relative to those of simpler states, as exciton state densities are rapidly increasing functions of the exciton numbers. These assumptions permit a simple closed form expression for the pre-equilibrium spectra in the

exciton model. The decay probability is computed as the sum over contributions from states with some initial exciton number n_0 to the equilibrium value $\bar{n}$. The master equation used for the exciton model is

$$dp(n,t)/dt = P(n-2,t)\left\langle \lambda_+^{n-2}(E)\right\rangle + P(n+2,t)\left\langle \lambda_-^{n+2}(E)\right\rangle - P(n,t)\left[\left\langle \lambda_+^{n}(E)\right\rangle + \left\langle \lambda_-^{n}(E)\right\rangle\right] \tag{6.1}$$

where $P(n,t)$ is the fraction of nuclei in the original ensemble which are in n exciton state at time t and $\left\langle \lambda_+^{n}(E)\right\rangle$ is the average inter nuclear transition rate from n exciton state going to $n+2$ exciton state; if the subscript is minus, transition rate is to $n-2$ exciton state.

The transition rates are evaluated on a relative basis as proportional to the average number of accessible final states. It predicts that as the energy becomes partitioned over an increasing number of degrees of freedom, the rate of high energy particle emission decreases many orders of magnitude from the maximum value. At lower excitation energies it predicts that the spectrum could be expressed as a prompt component plus an equilibrium component. The prompt component in this case extends beyond the definition of direct interaction. It reveals the fact that at higher excitation the nuclei may well decay prior to the attainment of statistical equilibrium. Performing the calculation with equation (6.1) on a time dependent basis, provides a single formulation that includes decay of the simple state following a direct reaction, decay of more complicated intermediate states, and decay of long lived equilibrium compound nucleus. The equidistance spacing model was used by Böhning [Bö70] for calculating the exact partial state densities that did not violate the Pauli Exclusion Principle. Much effort has been directed towards the calculation of either relative or absolute partial state lifetimes. Effects on rates due to the limitation of Pauli Exclusion Principle of densities of states [Ob74], or due to use of Fermi gas or harmonic oscillator potentials [Ga73], have been studied. Excitations where pre-equilibrium emission is likely to occur, the later considerations seem to be minor [Bl75].

6.1.2 Hybrid model

The exciton model is very simple and physically transparent in formulation. Only relative spectral shapes rather than absolute cross-sections could be calculated by this model. In order to solve this discrepancy, excited particle populations during equilibration were calculated by the use of partial state densities and inter nuclear transition rates of the excited particles were determined by calculating the mean free paths of the free nucleon-nucleon scattering cross-sections corrected for Pauli Exclusion Principle. This model was called hybrid model. The Pre-equilibrium decay probability in the hybrid model is given by [Bl73a], [Bl73b]

$$P_x(\varepsilon)d\varepsilon = \sum_{n=n_0}^{\bar{n}} \left[{}_n p_x \frac{\rho_{p,h}(U,\varepsilon) g d\varepsilon}{\rho_{p,h}(E)} \right] \left[\frac{\lambda_c(\varepsilon)}{\lambda_c(\varepsilon) + \lambda_+(\varepsilon)} \right] D_n \tag{6.2}$$

$$= \sum_{n=n_0}^{\bar{n}} {}_n P_x(\varepsilon) d\varepsilon$$

where

$P_x(\varepsilon)$ is the probability of emitting nucleon of type *x* with channel energy ε

${}_n P_x(\varepsilon)$ is the probability of emitting nucleon of type *x* with channel energy ε from *n* exciton state.

${}_n p_x$ is the number of *n* excitons that are nucleon type *x*.

$\rho_{p,h}(E) = \rho_n(E)$ is the density of *n* exciton state.

$\rho_{p,h}(U,\varepsilon)$ is the density of *n* exciton state such that one, if emitted, would have channel energy ε; differs from $\rho_{n-1}(U)$ by a factor $1/p$

D_n is the fraction of the reaction cross-section surviving decay prior to reaching the *n* exciton configuration.

$\lambda_c(\varepsilon)$ is the emission rate into the continuum of a particle of channel energy ε

$\lambda_+(\varepsilon)$ is inter nuclear transition rate of a particle at energy $\varepsilon + V$, where V is the real potential depth.

The expression in the first set of brackets uses partial state densities to give the number of particles of type *x* (neutrons and protons) in *n* exciton state that are in an unbound level with energy between ε and $d\varepsilon$ in the continuum. The second set of brackets gives the fraction of

those particles at energy ε that are emitted into the continuum rather than undergoing a transition to an n+2 exciton state. The D_n represents the population of the surviving particle emitted from simpler states.

By parameterization and simplification the hybrid model can be written as

$$\frac{d\sigma}{d\varepsilon} = \sigma_R / E \sum_{n=n_0}^{\bar{n}} \left[{}_n p_x (U/E)^{n-2} (n-1) \right] \{ D_n \sigma\varepsilon / gx / [\sigma\varepsilon / gx + 1890 \times (\varepsilon + BE_x) - 8(\varepsilon + BE_x)^2 \ ] \} \tag{6.3}$$

Here energies are in MeV and cross-section in mb [Bl73a], [Bl73b].

Due to the effect of entering the inter-nuclear transition rates in the formulation absolute cross-section calculated with pre-equilibrium models will have an error of first order which is linear with errors in $\lambda_+(\varepsilon)$. Energy dependent errors in inverse reaction cross-sections and partial state densities are also likely to be of greater influence than in equilibrium calculations.

Pre-equilibrium decay models have been formulated in terms of equilibration, predominantly by successive binary transitions. They provide a consistently good description of experimental results over a wide range of incident energies and projectile types. These models may be shown to provide a unified time-dependent description of nuclear reactions that includes direct, intermediate and equilibrium components.

6.1.3 Geometry-dependent hybrid model

In the analysis of nucleon induced reactions it was found that there is a major spectral contribution from the nuclear surface. To investigate the importance of nuclear density distribution on pre-equilibrium decay, the geometry-dependent hybrid model was formulated as [We73b]

$$\left(\frac{d\sigma}{d\varepsilon} \right) = \pi \lambda^2 \sum_{l=0}^{\infty} (2l+1) T_l \sum_{n=n_0}^{\bar{n}} {}_x P_n(\varepsilon) \tag{6.4}$$

The description of the parameter is the same as in the case of hybrid model. The density dependent parameters ${}_{x}P_{n}(\varepsilon)$ were averaged along the projectile paths corresponding to each partial wave. A Fermi density distribution function was used for this purpose. When the transition rate values of the particle from imaginary optical potential were used [Bl173a] the volume and surface form factors and parameters of Becchetti and Greenless [Be69] were applied. In the case of changes due to transition rate of the particle by nucleon-nucleon scattering due to density dependence of average cross-section and a change of velocity, the effect of the dependence of Fermi energy in local density approximation is very important. The hole energies cannot exceed the Fermi energy; partial state densities reflecting this limit will modify the exciton population of the equation (6.2).

6.2 Theoretical codes

For the comparison with the experimental data TALYS and AREL code has been used.

6.2.1 TALYS

TALYS has been developed in the HINDAS (High and Intermediate Energy Nuclear Data for Accelerator Driven System) project for complete and accurate simulation of nuclear reactions that involve neutrons, protons, deuterons, tritons and alpha particles, in the 1 keV-200 MeV energy range and for target nuclides of mass 12 and heavier.

For developing this code, the High Priority Request List of NEA [Ko98], has been used as a guide line.

The specific features of TALYS are

- In general an exact implementation of many of the latest nuclear models for direct, compound, pre-equilibrium and fission reactions.
- A continuous, smooth description of reaction mechanisms over a wide energy range (0.001-200 MeV) and mass number range ($12 < A < 339$).

- Completely integrated optical model and coupled-channels calculations by the ECIS-97 code [Ra94].
- Incorporation of recent optical model parameterizations for many nuclei
- Total and partial cross-sections, energy spectra, angular distributions, double-differential spectra and spectra.
- Discrete and continuum photon production cross-sections.
- Excitation functions for residual nuclide production, including isomeric cross-sections.
- An exact modelling of exclusive channel cross-sections, e.g. (n,2np), spectra, and recoils.
- Automatic reference to nuclear structure parameters as masses, discrete levels, resonances, level density parameters, deformation parameters, fission barrier and gamma-ray parameters, generally from the IEAA Reference Input Parameter Library [RIPL].
- Various width fluctuation models for binary compound reactions and at higher energies, multiple Hauser Feschbach emission until all reaction channels are closed.
- Various phenomenological and microscopic level density models.
- Various fission models to predict cross-sections and fission fragments and product yields.
- Models for pre-equilibrium reactions, and multiple pre-equilibrium reactions up to any order.
- Use of systematic if an adequate theory for a particular reaction mechanism is not yet available or implemented, or simply as a predictive alternative for more physical nuclear models.
- Automatic generation of nuclear data in ENDF-6 format.
- A transport source program.
- Easy input/output communication.
- An extensive user manual.
- A large collection of sample cases.

A particle incident on a target nucleus will induce several binary reactions which are described by the various competing reaction mechanisms. The end products of the binary reaction are the emitted particle and the corresponding recoiling residual nucleus. In general this is, however, not the end of the process. A total nuclear reaction may involve a whole

sequence of residual nuclei, especially at higher energies, resulting from multiple particle emission. All these residual nuclides have their own separation energies, optical model parameters, level densities, fission barriers, gamma-strength functions, etc., that must properly be taken into account along the reaction chain. The implementation of this entire reaction chain forms the backbone of TALYS. The program has been written in a way that enables a clear and easy inclusion of all possible nuclear model ingredients for any number of nuclides in the reaction chain. In this whole chain the target and primary compound nucleus have a special status, since they are subject to all reaction mechanisms, i.e. direct, pre-equilibrium, compound and fission and at low incident energies, width fluctuation corrections in compound nucleus decay.

The default local and global optical models that are used in TALYS are quite powerful mostly for (nearly) spherical nuclides. Although TALYS already have the full flexibility to use any deformed potential one wants as specific input, it has extended the optical model database for deformed nuclides as well. The same holds for light nuclides $A < 24$. Though TALYS describes a lot of possible features for the future, the code has been released in 2004 and is compared with this work. For more description about TALYS one is referred to [Ko04]

6.2.2 AREL

AREL is a relativistic version of the ALICE LIVERMORE code. It uses relativistic kinematics and includes pre-equilibrium emission up to two pre-compound particles per interaction and allows calculation for proton energies up to 900 MeV. However the code does not consider meson production, giant resonances, fragmentations or medium-energy fission. Due to internal limitations of array sizes, the calculations are restricted to product nuclides with atomic and mass numbers differing not more than 9 and 22 respectively, from those of the target nucleus for p-induced reactions [Bl83].

6.3 Discussions

The excitation function for a nuclear reaction exhibits many interesting features. There are different numbers of maxima at low energies due to different Q values followed by a continuum at intermediate energies. The broad peak at lower energies is due to the compound nuclear reaction, when the incident particle is absorbed by the nucleus, which then shares their energy with the nucleon inside the nucleus and finally the nucleus reaches statistical equilibrium. The increase in cross-section with proton energy indicates that the nucleus is in favourable position of capturing the incident particles. At low energy the density levels are low inside the target nucleus and the target nucleus can adjust the incident particle energy by continuous exchange of energy between different quantum state. The distribution of energy at this stage is symmetric about 90° usually with little angular distribution. At this point it has the characteristics of Maxwellian energy distribution [Ho82]. The decline of cross-section value indicates that further reaction channel is opening up. This means other competing reactions are activated and the probability for a particular reaction is decreased. The continuum part at intermediate energies is much less well understood. The continuum is partly due to direct process and partly due to pre-compound reaction that is, it also contains a component at the exit channel due to the particles emitted after direct process and before the final statistical equilibrium state is achieved. Pre-equilibrium particles are emitted in forward direction and are more energetic than the particles from the compound nucleus. The analysis of fluctuation in the cross-section as a function of energy specifies their presence. These fluctuations provide a measure of the interaction time and shows that these are the processes taking place in times intermediate between those taken by the direct process (transit time $\approx 10^{-22}$ to 10^{-23} sec) and by the decay of the compound nucleus ($\approx 10^{-16}$ sec).

The different theories in chapter 6.1 formulate the pre-equilibrium reaction. This will help in order to understand the comparison in the following sections.

6.3.1 Discussions for the excitation function $^{nat}W(p,xn)^{184}Re$

The experimentally obtained data were compared with previous work of Ullah [Ul04] as well as the theoretical codes TALYS and AREL. The gamma-energy line considered here is at 894.9 keV.

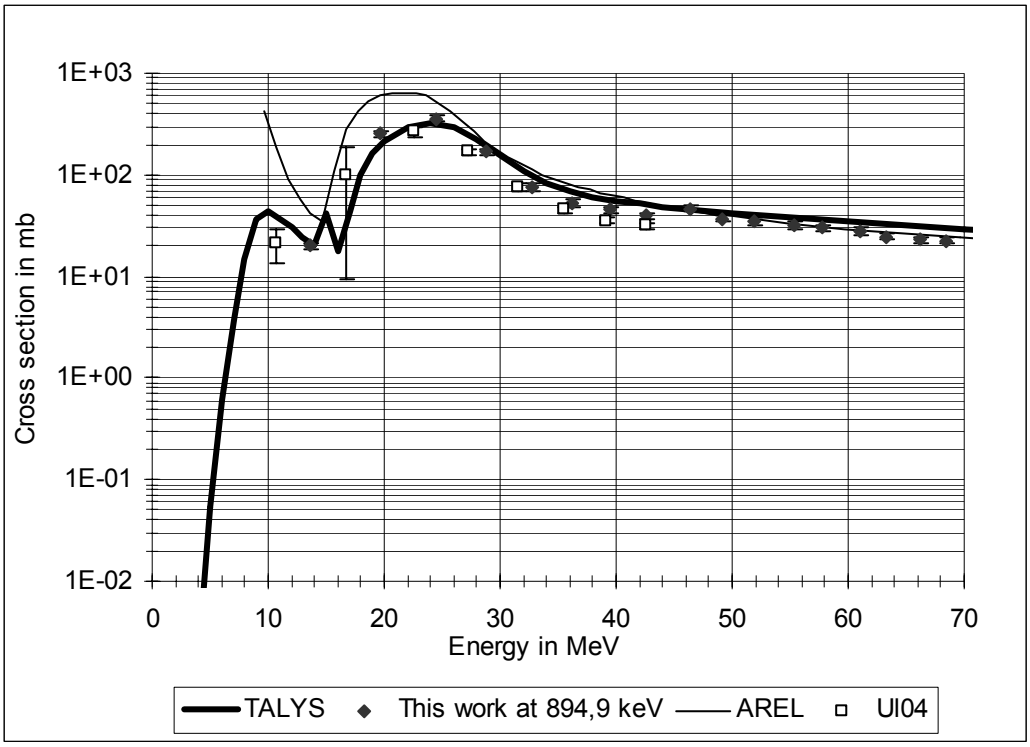

Fig. 6.1: Comparison of the experimentally obtained data for the reaction $^{nat}W(p,xn)^{184}Re$ with different theoretical models

The excitation function has two apparent maxima followed by a plateau. The maximum corresponds to compound reaction where the plateau is due to the pre-compound reaction. The excitation function for the reaction $^{nat}W(p,xn)^{184}Re$ is formed by the reaction $^{184}W(p,2n)^{184}Re$ with Q value -3.6 MeV which is not resolved in the experimental data as this value is lower than Coulomb threshold and $^{186}W(p,3n)^{184}Re$ with Q value -16.5 MeV which is evident. TALYS shows much agreement with experimental result than AREL in the low energy. There is a peak at 14.6 MeV in TALYS which is common for all the results. This is due to some numerical mistakes in TALYS which should be corrected. At lower energy AREL has a much higher value. At high energy AREL shows more consistency with the experimental data where TALYS is higher by a factor of one. This work also shows consistency with Ullah's [Ul04] work.

6.3.2 Discussions for the excitation function $^{nat}W(p,xn)^{182}Re$

Previous work of Ullah [Ul04] and Protoschill [Pr97a] as well as the theoretical codes are used for the comparison. The gamma-energy line considered is at 1221.4 keV

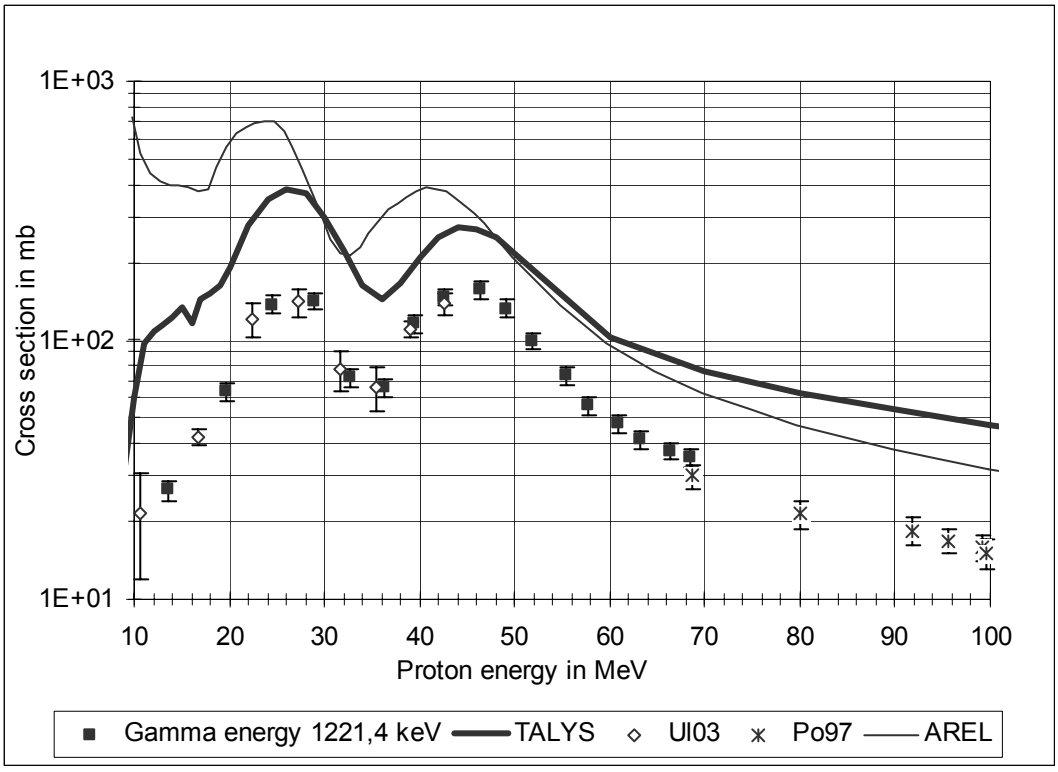

Fig. 6.2: Comparison of the experimentally obtained data for the reaction $^{nat}W(p,xn)^{182}Re$ with different theoretical models

The excitation function $^{nat}W(p,xn)^{182}Re$ is formed by four competitive reaction. They are $^{182}W(p,n)^{182}Re$ with Q value -3.6 MeV, $^{183}W(p,2n)^{182}Re$ with Q value -11.2 MeV, $^{184}W(p,3n)^{182}Re$ with Q value -17.2 MeV and $^{186}W(p,5n)^{182}Re$ with Q value -30.2 MeV. In fig. 6.2 it is observed that the excitation function is composed of two apparent maxima followed by a plateau. The maxima are due to the compound reaction and plateau due to pre-compound reaction. The maxima for the reaction $^{182}W(p,n)^{182}Re$ is not apparent as it is hindered by Coulomb thershold. The first maxima in fig. 6.2 is due to $^{183}W(p,2n)^{182}Re$. The region corresponding to the reaction $^{184}W(p,3n)^{182}Re$ also lies in this neighbourhood region of the second maxima as this is not clearly apparent due to low isotopic abundance. The second maxima corresponds to the reaction $^{186}W(p,5n)^{182}Re$. It is seen that at low energy the data of this work is in good agreement with [Ul04] and at high energy with [Pr97a]. But all the data

are below than TALYS and AREL. At energy 10.7 MeV TALYS is nearly in agreement with Ullah's work [Ul04]. But after that the values of TALYS is much higher while Ullah's work is in accordance to this work. The result from AREL is much higher than TALYS in this energy region. The maxima are at 28.83 MeV and 46.42 MeV. TALYS and AREL is higher by a factor of three and six respectively for the first maxima where a factor of two and four in the case of second maxima respectively. Then there is a gradual decline. This work coincides with the work of Protoschill [Pr97a] at 68.42 MeV. The results from TALYS and AREL are in agreement from 42 to 60 MeV. After 60 MeV AREL has lower value than TALYS. For the compound nucleus reaction at low energy TALYS appears to be better than AREL while in pre-equilibrium region AREL has close value with the experimental data than TALYS. The peak due to numerical mistakes at 14.6 MeV in TALYS is also present here.

6.3.3 Discussions for the excitation function $^{nat}W(p,xn)^{181}Re$

Only Protoschill's work [Pr97a] was available as well as with the theoretical codes for the comparison. The gamma energy line considered here is at 365.57 keV

The excitation function $^{nat}W(p,xn)^{181}Re$ is formed by the reactions $^{182}W(p,2n)^{181}Re$ with Q value -11.2 MeV, $^{183}W(p,3n)^{181}Re$ with Q value -19.2 MeV, $^{184}W(p,4n)^{181}Re$ with Q value -24.8 MeV and $^{186}W(p,6n)^{181}Re$ with Q value -37.8 MeV. The first maxima is due to $^{182}W(p,2n)^{181}Re$, while $^{183}W(p,3n)^{181}Re$ and $^{184}W(p,4n)^{181}Re$ lies in the region of the second maxima. They are not resolved individually as ^{184}W has a low isotopic aboundance and the third maxima correspond to the reaction $^{186}W(p,6n)^{181}Re$. TALYS shows better agreement with the experimental data than AREL. At 14.6 MeV TALYS shows the same problem of numerical mistake. Protoschill's [Pr97a] work at high energy is in well agreement with TALYS.

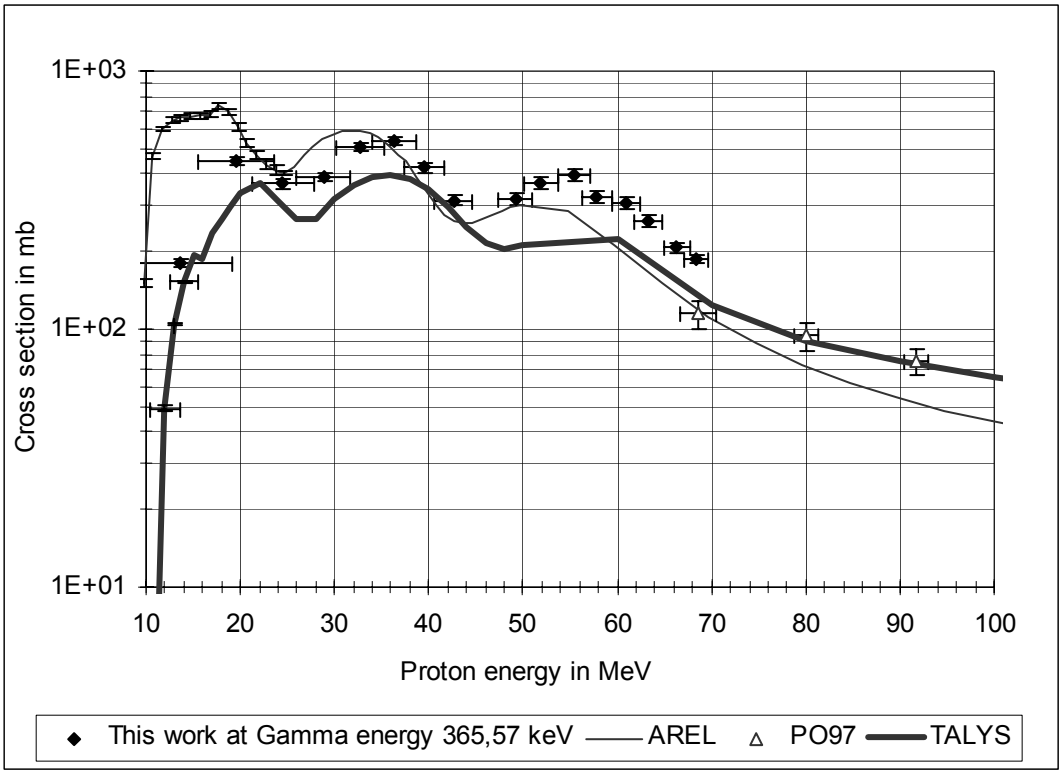

Fig. 6.3: Comparison of the experimentally obtained data for the reaction $^{nat}W(p,xn)^{181}Re$ with different theoretical models

6.3.4 Discussions for the excitation function $^{nat}W(p,2pxn)^{177}Ta$

No experimentally obtained data was available for the comparison. Thus it was compared only with theoretical codes. The gamma-energy line for which the excitation function was evaluated is at 112.94 keV. While the only other gamma-energy line at 208 keV for ^{177}Ta was not possible to identify due to low gamma-abundance.

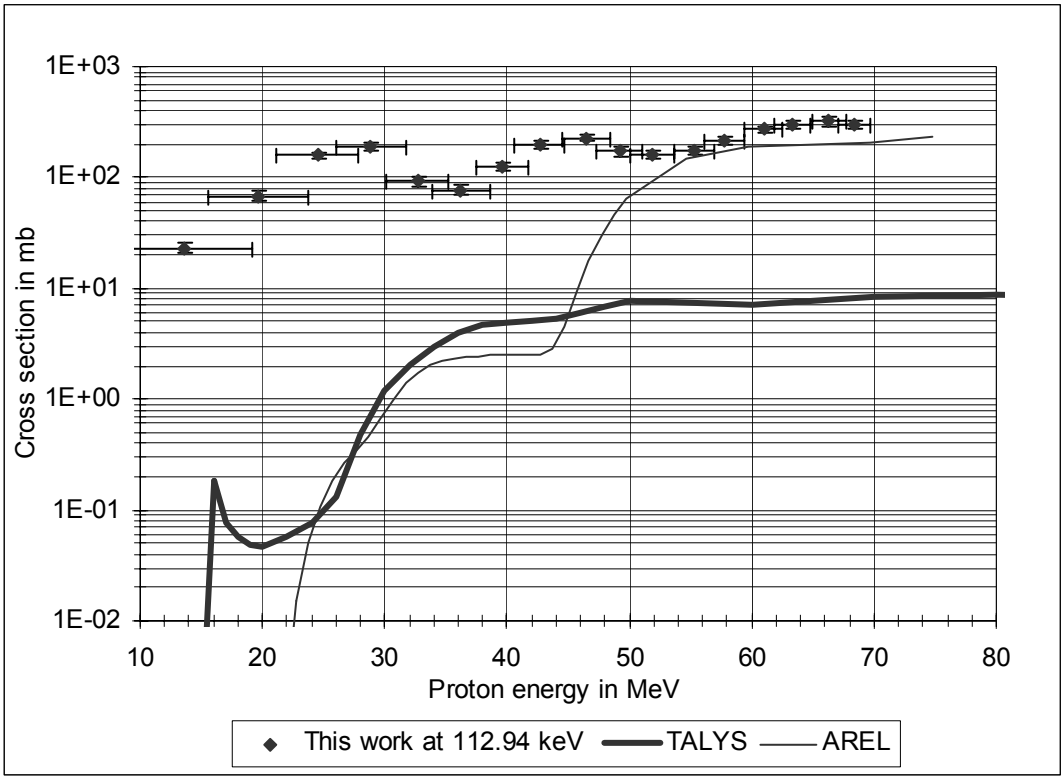

Fig. 6.4: Comparison of the experimentally obtained data for the reaction $^{nat}W(p,2pxn)^{177}Ta$ with different theoretical models

The excitation function can be formed in two different ways. That is either by emitting an alpha particle through the exit channel or emitting particle individually. For alpha particle in the exit channel the excitation function is formed by the reactions

$^{182}W(p,\alpha 2n)^{177}Ta$ with Q = -7.8 MeV

$^{183}W(p,\alpha 3n)^{177}Ta$ with Q = -14.0 MeV

$^{184}W(p,\alpha 4n)^{177}Ta$ with Q = -21.4 MeV

$^{186}W(p,\alpha 6n)^{177}Ta$ with Q = -34.3 MeV

For individual particle in the exit channel the excitation function is formed by the reaction

$^{182}W(p,2p4n)^{177}Ta$ with Q = -36.1 MeV
$^{183}W(p,2p5n)^{177}Ta$ with Q = -42.3 MeV
$^{184}W(p,2p6n)^{177}Ta$ with Q = -49.7 MeV
$^{186}W(p,2p8n)^{177}Ta$ with Q $\approx$ -62.6 MeV

Both of the models do not reveals any of these two kinds of phenomenon. In fact these models cannot be explained with the underlying physics.

Conclusions

The context of this work describes residual nuclides produced from tungsten by proton induced reaction. This was a part of the 5th frame work of the European Commission's project HINDAS (High and Intermediate Energy Nuclear Data for Accelerator Driven System). The goal of this project is to provide reliable nuclear reaction data for the feasibility studies of accelerator driven system. These data can further be used in evaluating new codes for nuclear reactions.

Irradiation of the target was performed at the PSI (Paul Scherrer Institute), Villigen, Switzerland using stacked foil technique. The energy range covered in this experiment was approximately from 10 MeV to 70 MeV. The samples were measured by off-line gamma-spectroscopy at the Center for Radiation Protection and Radioecology, University of Hannover. The spectrums were evaluated by commercially available software GAMMA-W in interactive mode.

Four radionuclides ^{184}Re, ^{182}Re, ^{181}Re and ^{177}Ta were identified from natural tungsten with a half-life between 19.9 hours and 67 days. Altogether 67 cross-sections were determined.

The evaluation was performed by different gamma-energy line for different radionuclides except for ^{177}Ta. The consistency of the results confirmed the validity of the measurement. For ^{177}Ta there was no other detectable gamma-energy line available.

The experimentally obtained data were compared with previously obtained experimental data and codes AREL and TALYS based on theoretical models. Good agreement between different experimental work and the codes were obtained for different isotopes of Re. Still in some cases there are discrepancy between the experimentally obtained data and the codes which require further improvements.

In the case of ^{177}Ta, there was no previously obtained data available. There are two processes by which the reaction ^{nat}W(p,2pxn)^{177}Ta can be performed. One is by the emission of alpha particle at the reaction channel and the other is by the emission of individual particles. None of the phenomenon is prevailed by the two theoretical codes TALYS and AREL. Much attention should be taken for the theoretical codes for this reaction. Further it would be

interesting to perform another experiment on tungsten at medium energy to check this reaction.

The gamma abundances taken from different nuclear libraries show consistency among themselves except in the case of ^{181}Re. This can be checked by performing another experiment on tungsten at this energy range.

This experiment produces a new set of cross-section data for tungsten. These data will extend cross-section library and will contribute to develop new and improved simulation codes.

References

[An77] Andersen H.H., Ziegler J.F., Hydrogen Stopping Powers and Range in All Elements, Vol.3 of The Stopping and Ranges of Ions in Matter, Pergamon Press, ISBN 0-08-021605-6, (1977)

[Be69] Becchetti F.D., Greenless G.W., 1969, Phys. Rev., 182:1190.

[Be01] Benlliure J., et al., Isotopic production cross-sections of fissions residues in ^{197}Au on proton collisions at 800A MeV, Nucl. Phys. A 638 (2001) 513-539.

[Bi95] BIPM, IEC, IFCC, ISO, IUPAC, IUPAP, OIML, Guide to the Expression of Uncertainty in Measurement 1995

[Bl73a] Blann M., 1973 Nucl. Phys. A 213:570

[Bl73b] Blann M., Winter Meet, Nucl. Phys. 9th Villars, 1973, ed. Milan Iorro I., Univ. Milan. Reproduced copy.

[Bl75] Blann, M. Pre-equilibrium Decay, Ann. Rev. Nucl. Sci. 25 (1975) 123

[Bl83] Blann M. and Vonach K., Phys. Rev. C 28 (1983) 1475

[BN04] Brook Haven National Laboratory (2004)
http://www.nndc.bnl.gov/

[Bo15] Bohr N., Philos. Mag. 30(1915) 581

[Bo92] Bowman, C.D., Arthur E.D., Lisowski P.W., Lawrence G.P, Jensen R.J., Anderson J.L., Blind B., Cappiello M., Davidson J.W., England T.R., Engel L.N., Haight R.C., Hughes H.G., Ireland J.R., Krakowski R.A., LaBauve R.J., Letellier B.C., Perry R.T., Russell G.J., Staudhammer K.P., Versamis G., Wilson W.B., Nuclear energy generation and waste transmutation using an

accelerator-driven intense thermal neutron source, Nucl. Instr. Meth. Phys. Res. A320 (1992) 336

[Bö70] Böhning M., 1970, Nucl. Phys. A 152:529

[Bu95] Busemann R., Michel R.,et al, TSL Progress Report 1994-1995, 1996 p. 36-38.

[Ca93] Caraminati F., Klapish R., Revol J.P., Roche Ch., Rubio J.A., and Rubbia C., An Energy Amplifier for Cleaner and Inexhaustible Nuclear Energy Production Driven by a Particle Beam Accelerator, CERN/AT/93-47(ET)(1993)

[Ch99] Chu S.Y.F., Ekström L.P., Firestone R.B., The Lund /LBNL Nuclear Data Search, LBNL Berkeley, U.S.A. and Department of Physics, Lund University, Sweden, 1999.
http://www.nucleardata.nuclear.lu.se/nucleardata/toi/radsearch.asp/

[En99] Enqvist T., et al., 1999, Symmetric experimental survey on projectile fragmentation and fission induced in collisions of ^{238}U at 1 A GeV with lead, Nucl. Phys. A 658 47-66.

[En01] Enqvist T., et al., Isotopic yields and kinetic energies of primary residues in A GeV ^{208}Pb + p reactions, Nucl. Phys. A 686 (2001) 481-524.

[En02] Enqvist T., et al., Primary residue production cross-sections and kinetic energies in 1 A GeV ^{208}Pb on deuteron reactions, Nucl. Phys. A. 703 (2002) 435-465.

[Fa97] Farget F., Benlliure J., Enqvist T., Taieb J., Schmidt K. H., Armbruster P., Bernas M., Mustapha B., Stephan C., Tassan-got L., Boudard A., Leray S., Legrain R., Volant C., Dufour J.P., Czajkowski S., Pravikoff M., Spallation reaction cross-sections relevant for accelerator-driven system, GSI Annual Report (1997)

[Fe74] Feshbach H., 1975, Rev. Mod. Phys. 46:1

[Fi96] R.B. Firestone and Shirley V.S., Eds., in: Table of Isotopes, 8 Ed., Wiley, New York, (1996)

[Gr66] Griffin J.J., 1966. Phys. Rev. Lett.17:478

[Gr67] Griffin J.J., 1967. Int. Nucl. Phys. Conf. 1966, Gatlinburg, Tenn., ed. Becker R.L., p.778. New York Academic

[Gr68] Griffin J.J., 1968. Intermediate Structure in Nuclear Reactions, ed. Kennedy H.P., Schrils R., Lexington: Univ. Kentucky Press. 219 pp.

[Gu69] Gunik R., Niday J.B., Anderson R.P., Meyer R.A., Gamma-ray energies and intensities, UCID-15439(1969)

[Ga73] Gadioli E., Gadioli-Erba E., Sona P.G., 1973, Nucl. Phys. A 217:570

[Gl98] Gloris M., PhD Thesis, University of Hannover, 1998

[Gl99] Gloris M., Michel R., Sudbrock F., Herpers U., Malmborg P., Holmqvist B., Proton-Induced Production of Residual Radionuclides in Lead at Intermediate Energies, Submitted to Nucl. Instr. Meth. Phys. Res. A (November 1998); Revised (February 1999)

[Ho82] Hodgson P.E., Pre-equilibrium processes in nuclear reactions. Opening address to the Varenna Conference on Nuclear Reaction Mechanisms Varenna Italy Jume. 1982.

[Ju86] Judith F. Briesmeister, (editor), MCNP (Monte Carlo Neutron and Proton Transport), Los Alamos National Laboratory Report LA 7396-M, Rev. 2 (1986).

[Ke73] Keller K.A., Lange J., Münzel H., LANDOLT-BÖRNSTEIN, Numerical Data and Functional Relationships in Science and Technology, New series, Editor in Chief: Hellwege, GroupI: Nuclear and Particle Physics, Volume 5, Q-Values

and Excitation Functions of Nuclear Reactions, Part A, Q-Values, Editor: Schopper H., Springer-Verlag Berlin. Heidelberg. NewYork,1973.

[Kl00] Klapisch R., Accelerator Driven Systems: An application of proton accelerators to nuclear power industry, Euro physics News (2000) Vol.31 No.6

[Kn00] Radiation Detection and Measurement, 3rd Edition, 2000, John Willey and Sons.U.S.A.

[Ko91a] N.P. Kocherov, Ed., Intermediate Energy Nuclear Data For Applications, INDC(NDS)-245 (1991)

[Ko98] Koning A. J., Delaroche J.-P., and Bersillon O., Nucl. Inst. Meth. A 414,49 (1998).

[Ko03] Koning A.J., Delaroch, Nucl. Phys. A 713,231(2003)

[Ko04] Koning A.J., Hilaire S., and Duijvestijn M.C., "TALYS: Comprehensive nuclear reaction modeling", *Proceedings of the International Conference on Nuclear Data for Science and Technology - ND2004*, Sep. 26 - Oct. 1, 2004, Santa Fe, USA,

[Mi73] Miller J.M., 1973, Proc Int. Conf. Nucl. Phys. Munich, ed. DeBoer J.J., Mang H.J., 2:597. Amsterdam: North-Holland

[Mi 97a] Michel R., Bodemann R., Busemann H., R. Daunke, M. Gloris, Lamge H.-J., Klug B., Krins A., Leya I., Lüpke M., Neumann S., Reinhardt H., Schnatz-Büttgen M., Herpers U., Hannen Th., Kubik P.-W., Synal H. -A., Cross-sections for the Production of Residual Nuclides by Low and Medium-Energy Protons from the Traget Elements C, N, O, Mg, Ca, Ti, Al, Si, Mn, Fe, Co, Ni, Cu, Sr, Y, Zr, Nb, Ba, and Au. Nucl. Inst. Meth. in Phys. Res. B. 129 (1997) 153-193.

[Mi97b] Michel R., et al., Nucl. Int. Meth. B-129 (1997) 153.

[Mi97c] Michel R., Proc. GEDEON, Gestion des Dechets par des Options Nouvelles, Experimental Spallation Studies for the Transmutation of Nuclear Waste: Present and Future, Scalay, 24.01.1997

[Ob74] Oblozinsky P., Ribansky I., Betak E., 1974, Nucl. Phys. A 226:347

[Pa68] Palms J.M. et al., Nucl. Instrum.Meth.64, 310 (1968)

[Ph70] Philippot J. Cl., IEEE Trans. Nucl. Sci. NS-17(3), 446(1970)

[Pr97a] Protoschill J., Untersuchung der Restkernproduktion durch protoneninduzierte Reaktionen an schweren Targetelementen, Diplomarbeit, Universität Hannover (1997)

[Qa 97] Qaim S.M., Radioactivity in Medicine: Achievements, Perspectives and Role of Nuclear Data, in: Reffo G., Ventura A., Grandi C. (eds.), Proc. Int. Conf. Nuclear Data for Science and Technology, Trieste, 19-24 May 1997, IPSConf. Proc. 59 Bologna (1997) 31

[Ra94] Raynal J., Notes on ECIS94, CEA Saclay Report No. CEA-N-2772, 1994

[Re83] Reuss U., Westmeier W., At. Data Nucl. Data Tables 29 (1983)

[Re01] Rejmund F., et al., Measurement of isotopic cross-sections of spallation residues in 800 A MeV ^{197}Au + p collisions, Nucl. Phys. A 638 (2001) 540-565.

[Ri89] Richard E. Prael and Henry Lichenstein, LA-UR-89-3014, Los Alamos National Laboratory (1989).

[RIPL] Handbook for calculations of nuclear reaction data: Reference Input Parameter Library, http://www.nds.iaea.or.at/RIPL-2/.

[Ru95] Rubbia C., Rubio J.A., Buono S., Carminati F., Fietier N., Galvez J., Geles C, Kadi Y., Klapisch R. , Mandrillon P., Revol J.P., Roche Ch., Conceptual Design of a Fast Neutron Operated High Power Energy Amplifier, CERN/AT/95-44(ET)

[Se47] Serber R., Nuclear Reactions at High Energies, Phys. Rev. 72 (1947) 1114

[Tr92] TRIM version 92.16, Ziegler J.F. and Biersack J.F., Updated version of a computer code for calculating Stopping and Ranges

[Ul04] Ullah Z., Medium Energy Cross-sections for the Production of Residual Nuclides Relevant for Accelerator Driven Technology, Diploma Thesis, University of Hannover, 2004

[We37a] Weisskopf V.F., Statistics and Nuclear Reactions, Phys. Rev. 52 (1937) 295

[We37b] Weisskopf V.F., 1937, Phys. Rev. 53:295

[We94] Westmeier W., Commercially available code GAMMA-W, Ver. 15.03 (1994)

[We95] Westmeier W., GAMMA-W Manual, (1995)

[Wi71] Williams F.C. Jr., 1971, Nucl. Phys. A 166: 231

[Wi80] Wilson W.B., England T.B., La Bauve R.J., Battat M.E., Wessel D.E., Perry R.T., Los Alamos Report LA-UR80-2107 (1980)

[Zi85] Ziegler J.F., Biersack J.P., Littmark U., The Stopping Power and Range of Ions in Solids, Vol. 1 of the Stopping and Ranges of Ions in Matter, Pergamon Press, New York, 1985.

[Zu69] Zulliger H.R., Middleman L.M. and Aitken D.W., IEEE Trans. Nucl. Sci. NS-16(1), 47 (1969)

Appendix

Table A.1: Cross-sections data for the reaction $^{nat}W(p,xn)^{184}Re$ at E_γ = 792.07 keV with I_γ = 0.375 [Ch99].

Target	Reaction	Product	E_p in MeV	u(Ep) in MeV	σ in mb	u(σ) in mb
^{nat}W	p,xn	^{184}Re	68.42	1.33	2.21E+01	9.91E-01
^{nat}W	p,xn	^{184}Re	66.27	1.39	2.27E+01	9.22E-01
^{nat}W	p,xn	^{184}Re	63.27	1.46	2.41E+01	1.12E+00
^{nat}W	p,xn	^{184}Re	60.98	1.51	2.64E+01	1.36E+00
^{nat}W	p,xn	^{184}Re	57.79	1.61	2.87E+01	1.71E+00
^{nat}W	p,xn	^{184}Re	55.34	1.68	3.29E+01	3.30E+00
^{nat}W	p,xn	^{184}Re	51.88	1.78	3.45E+01	2.34E+00
^{nat}W	p,xn	^{184}Re	49.20	1.87	3.65E+01	6.81E-01
^{nat}W	p,xn	^{184}Re	46.42	1.97	4.64E+01	1.30E+01
^{nat}W	p,xn	^{184}Re	42.64	1.99	3.71E+01	2.19E+00
^{nat}W	p,xn	^{184}Re	39.54	2.14	4.46E+01	9.26E-01
^{nat}W	p,xn	^{184}Re	36.23	2.33	5.16E+01	1.01E+00
^{nat}W	p,xn	^{184}Re	32.68	2.57	7.39E+01	5.32E-01
^{nat}W	p,xn	^{184}Re	28.83	2.88	1.64E+02	2.85E+00
^{nat}W	p,xn	^{184}Re	24.52	3.33	3.54E+02	6.98E+00
^{nat}W	p,xn	^{184}Re	19.62	4.07	2.51E+02	2.18E-01
^{nat}W	p,xn	^{184}Re	13.54	5.64	1.98E+01	1.47E-01

Table A.2: Cross-sections data for the reaction $^{nat}W(p,xn)^{184}Re$ at E_γ = 903.3 keV with I_γ = 0.379 [Ch99].

Target	Reaction	Product	E_p in MeV	u(Ep) in MeV	σ in mb	u(σ) in mb
^{nat}W	p,xn	^{184}Re	68.42	1.33	2.21E+01	9.24E-01
^{nat}W	p,xn	^{184}Re	66.27	1.39	2.28E+01	1.23E+00
^{nat}W	p,xn	^{184}Re	63.27	1.46	2.43E+01	9.45E-01
^{nat}W	p,xn	^{184}Re	60.98	1.51	2.68E+01	6.20E-01
^{nat}W	p,xn	^{184}Re	57.79	1.61	2.93E+01	1.11E+00
^{nat}W	p,xn	^{184}Re	55.34	1.68	3.06E+01	3.55E+00
^{nat}W	p,xn	^{184}Re	51.88	1.78	3.46E+01	5.77E+00
^{nat}W	p,xn	^{184}Re	49.20	1.87	3.66E+01	6.51E-01
^{nat}W	p,xn	^{184}Re	46.42	1.97	4.63E+01	1.20E+01
^{nat}W	p,xn	^{184}Re	42.64	1.99	3.82E+01	5.93E-01
^{nat}W	p,xn	^{184}Re	39.54	2.14	4.48E+01	7.81E-01
^{nat}W	p,xn	^{184}Re	36.23	2.33	5.18E+01	7.13E-01
^{nat}W	p,xn	^{184}Re	32.68	2.57	7.42E+01	5.36E-01
^{nat}W	p,xn	^{184}Re	28.83	2.88	1.65E+02	2.20E+00
^{nat}W	p,xn	^{184}Re	24.52	3.33	3.52E+02	9.16E+00
^{nat}W	p,xn	^{184}Re	19.62	4.07	2.50E+02	5.57E-02
^{nat}W	p,xn	^{184}Re	13.54	5.64	1.98E+01	1.59E-01

Table A.3: Cross-sections data for the reaction $^{nat}W(p,xn)^{182}Re$ at E_γ = 229.3 keV with I_γ = 0.26 [Ch99].

Target	Reaction	Product	E_p in MeV	u(Ep) in MeV	σ in mb	u(σ) in mb
^{nat}W	p,xn	^{182}Re	68.42	1.33	4.58E+01	2.08E+00
^{nat}W	p,xn	^{182}Re	66.27	1.39	4.97E+01	3.93E+00
^{nat}W	p,xn	^{1182}Re	63.27	1.46	5.64E+01	4.70E+00
^{nat}W	p,xn	^{182}Re	60.98	1.51	6.68E+01	2.63E+00
^{nat}W	p,xn	^{1182}Re	57.79	1.61	7.42E+01	1.30E+01
^{nat}W	p,xn	^{182}Re	55.34	1.68	1.02E+02	6.96E+00
^{nat}W	p,xn	^{182}Re	51.88	1.78	1.42E+02	1.05E+01
^{nat}W	p,xn	^{182}Re	49.20	1.87	1.88E+02	4.24E+00
^{nat}W	p,xn	^{1182}Re	46.42	1.97	1.97E+02	1.55E+01
^{nat}W	p,xn	^{182}Re	42.64	1.99	2.10E+02	1.26E+01
^{nat}W	p,xn	^{182}Re	39.54	2.14	1.67E+02	1.00E+01
^{nat}W	p,xn	^{182}Re	36.23	2.33	9.27E+01	4.41E+00
^{nat}W	p,xn	^{182}Re	32.68	2.57	1.03E+02	4.34E+00
^{nat}W	p,xn	^{182}Re	28.83	2.88	2.02E+02	1.10E+01
^{nat}W	p,xn	^{182}Re	24.52	3.33	1.81E+02	2.11E+01
^{nat}W	p,xn	^{182}Re	19.62	4.07	8.65E+01	9.07E+00
^{nat}W	p,xn	^{182}Re	13.54	5.64	3.53E+01	3.81E+00

Table A.4: Cross-sections data for the reaction $^{nat}W(p,xn)^{182}Re$ at E_γ = 1121.3 keV with I_γ = 0.22 [Ch99].

Target	Reaction	Product	E_p in MeV	u(Ep) in MeV	σ in mb	u(σ) in mb
^{nat}W	p,xn	^{182}Re	68.42	1.33	3.91E+01	4.96E+00
^{nat}W	p,xn	^{182}Re	66.27	1.39	3.67E+01	6.05E+00
^{nat}W	p,xn	^{1182}Re	63.27	1.46	3.80E+01	1.86E+01
^{nat}W	p,xn	^{182}Re	60.98	1.51	5.16E+01	6.27E+00
^{nat}W	p,xn	^{1182}Re	57.79	1.61	6.33E+01	8.66E+00
^{nat}W	p,xn	^{182}Re	55.34	1.68	8.23E+01	1.24E+01
^{nat}W	p,xn	^{182}Re	51.88	1.78	1.11E+02	1.51E+01
^{nat}W	p,xn	^{182}Re	49.20	1.87	1.42E+02	1.40E+01
^{nat}W	p,xn	^{1182}Re	46.42	1.97	1.70E+02	1.36E+01
^{nat}W	p,xn	^{182}Re	42.64	1.99	1.57E+02	1.38E+01
^{nat}W	p,xn	^{182}Re	39.54	2.14	1.22E+02	1.11E+01
^{nat}W	p,xn	^{182}Re	36.23	2.33	7.00E+01	6.75E+00
^{nat}W	p,xn	^{182}Re	32.68	2.57	7.68E+01	8.65E+00
^{nat}W	p,xn	^{182}Re	28.83	2.88	1.53E+02	1.74E+01
^{nat}W	p,xn	^{182}Re	24.52	3.33	1.50E+02	1.77E+01
^{nat}W	p,xn	^{182}Re	19.62	4.07	7.13E+01	7.30E+00
^{nat}W	p,xn	^{182}Re	13.54	5.64	3.06E+01	2.43E+00

Table. A.5: Cross-sections data for the reaction $^{nat}W(p,xn)^{181}Re$ at E_γ = 360.7 keV with I_γ = 0.12 [Re83].

Target	Reaction	Product	Ep in MeV	u(Ep) in MeV	σ in mb	u(σ) in mb
^{nat}W	p,xn	^{181}Re	68.42	1.33	1.87E+02	1.46E+01
^{nat}W	p,xn	^{181}Re	66.27	1.39	2.06E+02	2.12E+01
^{nat}W	p,xn	^{181}Re	63.27	1.46	2.63E+02	1.92E+01
^{nat}W	p,xn	^{181}Re	60.98	1.51	3.07E+02	2.28E+01
^{nat}W	p,xn	^{181}Re	57.79	1.61	3.24E+02	8.65E+01
^{nat}W	p,xn	^{181}Re	55.34	1.68	3.99E+02	3.03E+01
^{nat}W	p,xn	^{181}Re	51.88	1.78	3.67E+02	3.49E+01
^{nat}W	p,xn	^{181}Re	49.20	1.87	3.21E+02	2.15E+01
^{nat}W	p,xn	^{181}Re	42.64	1.99	3.16E+02	2.04E+01
^{nat}W	p,xn	^{181}Re	39.54	2.14	4.21E+02	2.39E+01
^{nat}W	p,xn	^{181}Re	36.23	2.33	5.34E+02	3.85E+01
^{nat}W	p,xn	^{181}Re	32.68	2.57	5.08E+02	3.99E+01
^{nat}W	p,xn	^{181}Re	28.83	2.88	3.88E+02	2.63E+01
^{nat}W	p,xn	^{181}Re	24.52	3.33	3.68E+02	1.51E+01
^{nat}W	p,xn	^{181}Re	19.62	4.07	4.48E+02	3.30E+01
^{nat}W	p,xn	^{181}Re	13.54	5.64	1.81E+02	1.44E+01

Table. A.6: Cross-sections data for the reaction $^{nat}W(p,xn)^{181}Re$ at E_γ = 639.3 keV with I_γ = 0.0645 [Ch99].

Target	Reaction	Product	Ep in MeV	u(Ep) in MeV	σ in mb	u(σ) in mb
^{nat}W	p,xn	^{181}Re	68.42	1.33	1.88E+02	5.28E+00
^{nat}W	p,xn	^{181}Re	66.27	1.39	2.08E+02	1.07E+01
^{nat}W	p,xn	^{181}Re	63.27	1.46	2.64E+02	1.35E+01
^{nat}W	p,xn	^{181}Re	60.98	1.51	3.09E+02	1.59E+01
^{nat}W	p,xn	^{181}Re	57.79	1.61	3.26E+02	1.91E+01
^{nat}W	p,xn	^{181}Re	55.34	1.68	4.01E+02	2.07E+01
^{nat}W	p,xn	^{181}Re	51.88	1.78	3.70E+02	1.94E+01
^{nat}W	p,xn	^{181}Re	49.20	1.87	3.23E+02	1.68E+01
^{nat}W	p,xn	^{181}Re	42.64	1.99	3.18E+02	1.60E+01
^{nat}W	p,xn	^{181}Re	39.54	2.14	4.24E+02	2.19E+01
^{nat}W	p,xn	^{181}Re	36.23	2.33	5.38E+02	2.14E+01
^{nat}W	p,xn	^{181}Re	32.68	2.57	5.11E+02	2.02E+01
^{nat}W	p,xn	^{181}Re	28.83	2.88	3.91E+02	1.52E+01
^{nat}W	p,xn	^{181}Re	24.52	3.33	3.70E+02	1.64E+01
^{nat}W	p,xn	^{181}Re	19.62	4.07	4.51E+02	1.75E+01
^{nat}W	p,xn	^{181}Re	13.54	5.64	1.82E+02	7.26E+00

Acknowledgement

Thanks to the Almighty Allah who enabled me to accomplished this work.

My thanks goes to my supervisor Professor Dr. Rolf Michel for providing me the opportunity to work with him. His continuous supervision and guidance made it very easy for me to complete the work. I was always welcome to him for any sort of problem. It was a real pleasure to work with him.

I am grateful to World Laboratory, Lausanne, Switzerland for providing a generous scholarship.

I would like to thank the technical staffs of the Paul Scherrer Institute for the irradiation experiment and Dr. U. Herpers, U. Otto and E. Bolz of the Department of Nuclear Chemistry , University of Cologne, for preparing the samples.

Thanks to Mr. R. Sachse for cooperating me with the laboratory work. I also thanks to Dr. M. Taschner and Mr. J. Lüdke for their assistancy regarding the computer.

Thanks to Mr. Z. Ullah for his encouragement and help during the work.

I am grateful to all the members of the ZSR for providing me a wonderful environment.

I would like to thank Dr. Aminul Islam for helping me in editing the thesis.

I am grateful to my parents and my fiancée Tammana for their moral support and continuous encouragement during the whole period of time.

Thanks

Abu Salek Md. Fahim Chowdhury